# Intruder structures observed in $^{122}$Te through inelastic neutron scattering

S. F. Hicks, G. K. Alexander, C. A. Aubin, M. C. Burns, C. J. Collard, and M. M. Walbran
*Department of Physics, University of Dallas, Irving, Texas 75062*

J. R. Vanhoy and E. Jensen
*Department of Physics, United States Naval Academy, Annapolis, Maryland 21402*

P. E. Garrett,[1] M. Kadi,[2] A. Martin,[1] N. Warr,[1] and S. W. Yates[1,2]
[1]*Department of Physics and Astronomy, University of Kentucky, Lexington, Kentucky 40506-0055*
[2]*Department of Chemistry, University of Kentucky, Lexington, Kentucky 40506-0055*
(Received 12 November 2004; published 15 March 2005)

The excited levels of $^{122}$Te to 3.3-MeV excitation have been studied using $\gamma$-ray spectroscopy following inelastic neutron scattering. The decay characteristics of these levels have been determined from $\gamma$-ray excitation functions, angular distributions at $E_n = 1.72$, 2.80, and 3.35 MeV, Doppler shifts, and $\gamma\gamma$ coincidences. Electromagnetic transition rates were deduced for many levels, as were multipole-mixing and branching ratios. Level energies and electromagnetic transition rates were compared to interacting boson model (IBM) calculations, both with and without intruder-state mixing, and to particle-core coupling model calculations. The energies of low-lying levels of $^{122}$Te are well described by the IBM with intruder-state mixing calculations, and observed transition rates support emerging intruder bands built on $0^+$ levels. The other models considered do not produce enough low-lying positive parity states; however, U(5) energies to the four quadrupole-phonon level agree very well with observations when states with large intruder configurations are ignored. Mixed-symmetry and quadrupole-octupole excitations have been investigated, but mixing with other configurations and fragmentation of strength prohibit a clear identification of these states.

DOI: 10.1103/PhysRevC.71.034307 PACS number(s): 25.40.Fq, 27.60.+j, 23.20.−g

## I. INTRODUCTION

The $^{122}$Te nucleus with two protons beyond the closed $Z = 50$ shell is expected to have excitations predominantly of vibrational character, although it has also been characterized as a $\gamma$ soft or O(6) nucleus [1]. Kern *et al.* [2] claim this nucleus is a good example of one exhibiting the U(5) dynamical symmetry, as was previously found in $^{118}$Cd, which mirrors $^{122}$Te with respect to the $Z = 50$ shell closure [3].

Identification of multiphonon excitations in $^{122}$Te and of the best dynamical symmetry to characterize this nucleus is complicated by the strong role played by 4p-2h intruder configurations [4,5] and by two-quasiparticle proton excitations [6–9]. Mixing between these configurations appears to play a stronger role in low-lying levels in the Te nuclei than in other nearby nuclei [8]. Past theoretical investigations of $^{122}$Te have been hampered by limited experimental information regarding the level scheme and decay characteristics of this nucleus, especially with regard to absolute electromagnetic transition rates. For example, intruder bands have been proposed from IBM-2 calculations [4], but no intraband transitions have previously been observed and B($E2$) values have not been determined to test model predictions.

In the present work involving $\gamma$-ray detection following inelastic neutron scattering, levels in $^{122}$Te with spins $J \leqslant 6$ below 3.3-MeV excitation were investigated. Lifetimes in the range of a few femtoseconds to approximately two picoseconds were determined using the Doppler-shift attenuation method (DSAM). Reduced electromagnetic transition rates were determined to investigate the aforementioned structures within the framework of the interacting boson model (IBM) and the particle-core coupling model (PCM). States of mixed neutron-proton symmetry and multiphonon quadrupole-octupole coupled states were also investigated. Several low-lying states with $J^\pi = 0^+$ were unambiguously identified for the first time, and, in general, the existing level scheme of $^{122}$Te [10] was found to be very deficient.

Previous information regarding the level structure of $^{122}$Te is compiled in Ref. [10]. More recent experimental investigations include the following: $^{122}$Te($d,d'$)$^{122}$Te, $^{123}$Te($d,t$)$^{122}$Te, $^{123}$Te($^3$He,$^4$He)$^{122}$Te, $^{121}$Sb($^3$He,$d$)$^{122}$Te, and $^{122}$Te($\gamma,\gamma'$)$^{122}$Te [5] and reactor ($n,n'\gamma$) [11,12] and ($\alpha,2n$) reactions [9]. Existing information is combined with new ($n,n'\gamma$) results to extend the detailed level information to 3.3 MeV in $^{122}$Te.

The experimental procedures and data reduction techniques used in these ($n,n'\gamma$) measurements are discussed in Sec. II. The level properties of states requiring special attention are given in Sec. III. Section IV is devoted to model discussions and special structures. Finally, results and conclusions are presented in Sec. V.

## II. EXPERIMENTAL METHOD AND DATA ANALYSIS

Measurements were made using the neutron scattering facilities at the University of Kentucky 7-MV electrostatic accelerator laboratory. The $^3$H($p,n$)$^3$He reaction was used as a neutron source. The 5.075-g powdered $^{122}$Te sample, isotopically enriched to 97.12%, was packed into a thin-walled

 

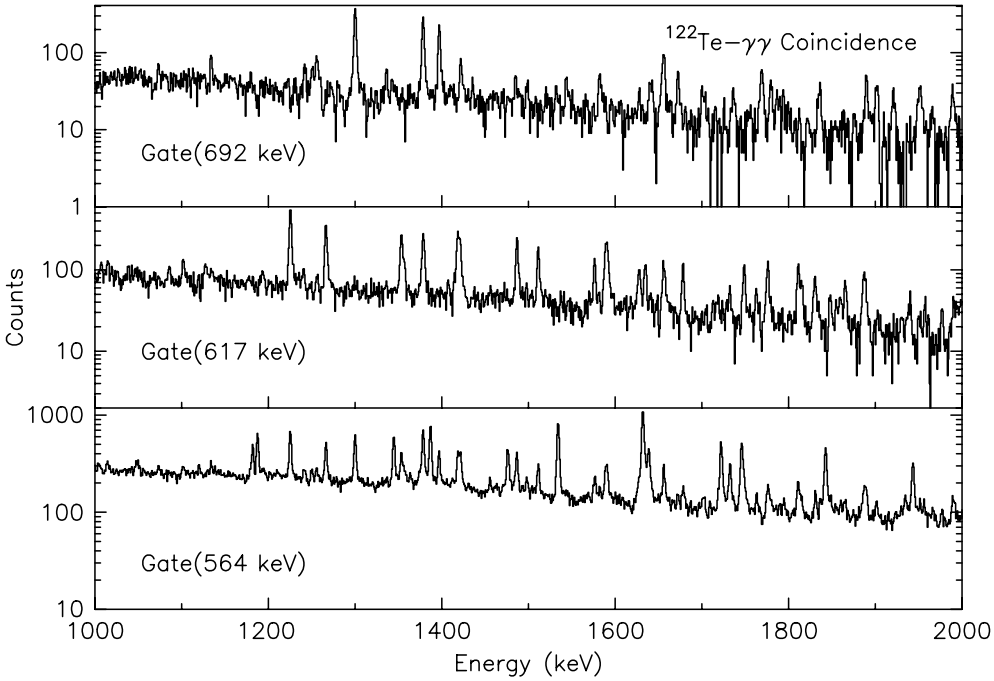


FIG. 1. Coincidence spectra from gates set on the 564.1-, 617.1-, and 692.7-keV $\gamma$ rays from the first, second, and third $^{122}$Te excited states, respectively, for $\gamma$-ray energies between 1000 and 2000 keV.

lucite container with a diameter of 1.42 cm and a height of 2.45 cm.

$\gamma$-$\gamma$ coincidences were measured at an incident neutron energy of 3.6 MeV. Neutrons emerging from the gas cell were formed into a 1-cm beam using a lithium-loaded collimator approximately 75 cm long. The sample was hung coaxially with the beam, and four high-efficiency HpGe detectors were placed in a coplanar arrangement approximately 6 cm from the center of the sample. Data were stored in event mode, and a two-dimensional matrix was constructed offline by considering pairwise coincidences. Portions of the coincidence spectra are shown in Fig. 1 for the 564-, 617-, and 692-keV gates. The experimental apparatus is discussed in detail in Ref. [13].

A singles target-detector configuration was used to measure $\gamma$-ray excitation functions, angular distributions, and Doppler shifts. $\gamma$ rays were detected using a Compton-suppressed *n*-type HpGe detector with 51% relative efficiency and an energy resolution of 2.1 keV FWHM at 1.33 MeV. Compton suppression was achieved using a BGO annulus detector surrounding the HpGe detector. The gain stability of the system was monitored using $^{56}$Co and $^{152}$Eu radioactive sources. The neutron scattering facilities, TOF neutron background suppression, neutron monitoring, and data reduction techniques have been described elsewhere [13,14].

Excitation functions, measured for incident neutron energies between 1.9 and 3.4 MeV in approximately 100-keV steps, were used to place $\gamma$rays in the level scheme, to determine level energies, and to assist in spin assignments. Figure 2 shows spectra at three different incident neutron energies. $\gamma$-ray yields from the excitation function measurements were corrected for $\gamma$-ray detection efficiency and were normalized to yields from the neutron monitor, whose yields were corrected for efficiency as a function of neutron energy to obtain relative $\gamma$-ray production cross sections. A normalization appropriate for interpreting cross sections was obtained by comparing statistical model calculations [15] and experimental cross sections for $0^+$ levels. These relative cross sections were then compared to theoretical values calculated with the statistical model code CINDY [15], using optical model parameters for this mass and energy region [16] to evaluate the consistency of the spin assignments and branching ratios determined from angular distribution measurements, as shown in Figs. 3 and 4, respectively. Levels to approximately 3 MeV that exhibit inconsistencies with the statistical model calculations are indicated by a *k* in Table I. Differences between the calculations and experiment indicate either missing decay strength, which affects the branching ratios, or states not adequately represented by a statistical interpretation.

$\gamma$-ray angular distributions were measured at incident neutron energies of 1.7, 2.8, and 3.4 MeV at five, eight, and nine angles, respectively. Level spins and multipole-mixing ratios were determined by comparing the measured angular distributions with calculations from the statistical model code CINDY [15] as discussed previously [17]. Sample $\gamma$-ray angular distributions are shown in Fig. 5. Figure 5(c) is an example of the $\chi^2$ versus $\tan^{-1}(\delta)$ used to determine the spin and multipole-mixing ratio for the transition shown in Fig. 5(a). Often two solutions for $\delta$ give similar values of $\chi^2$; the value of $\delta$ with the smaller $\chi^2$ is included in the table unless the state is discussed further in the paper, in which case both solutions are listed in Table I. Branching ratios were derived from the angular distribution data at the lowest incident neutron energy possible, unless otherwise noted.

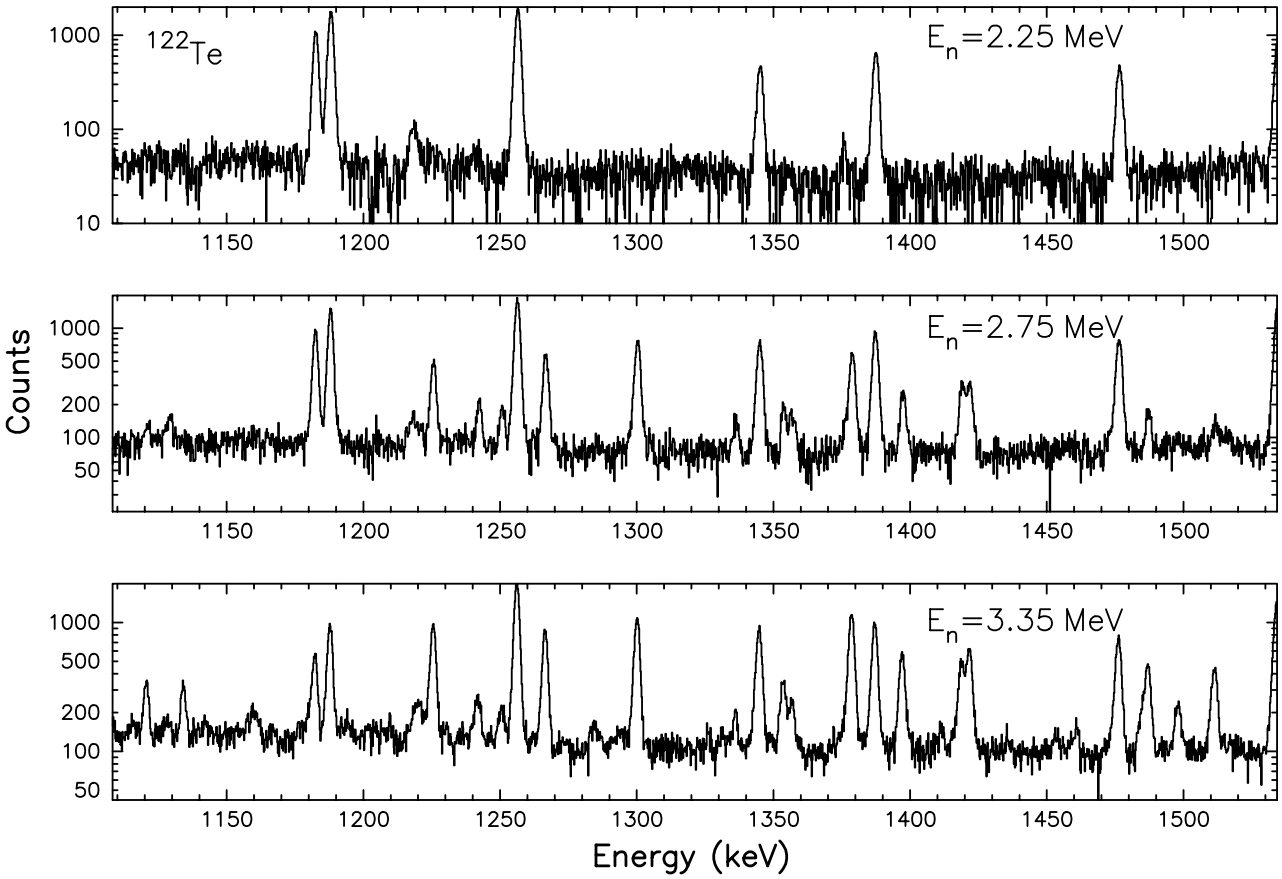


FIG. 2. Experimental spectra from $\gamma$-ray excitation function measurements at incident neutron energies of 2.25, 2.75, and 3.35 MeV.

Level lifetimes were extracted using DSAM following inelastic neutron scattering [18]. Lifetimes were determined by comparing experimental and theoretical Doppler-shift attenuation factors. Theoretical attenuation factors $F(\tau)$ were calculated using the stopping theory of Winterbon [19]. Mean lifetimes in the range of a few femtoseconds to approximately 2 ps were determined in this experiment. The Doppler shifts for several transitions, as well as theoretical $F(\tau)$ calculations for the 2719-keV $\gamma$ ray, are shown in Fig. 6.

Experimental information, including $\gamma$-ray intensities, $a_2$ and $a_4$ angular distribution coefficients, and transition energies, derived from the excitation functions and angular distributions for all observed levels, is available from the authors and will be submitted to the Nuclear Data Compilation Center.

## III. LEVEL DISCUSSION

Level energies, $\gamma$-ray placements, branching ratios, spin and parity assignments, multipole-mixing ratios, $F(\tau)$ values, lifetimes, and transition rates for all observed levels are given in Table I. Adopted levels and transitions [10] are indicated by an *a* in the note column of Table I. Most transitions and many levels observed were not previously adopted.

Adopted levels below 3.3 MeV not observed in this investigation include the following: (1) states of high spin typically not seen in $(n,n'\gamma)$ reactions, which are the 2669 $(8^+)$-, 2800 $(7^-)$-, 2913 $(8^+)$-, 3210 $(10^+)$-, and 3290 $(10^+)$-keV levels; (2) states with large energy spreads that may correspond to levels observed in this work, but for which the correspondence is not clear, that is, the 2549(13)-, 2665(13)-, 2740(24)-, 2780(24)-, 2790(24)-, 2940(15)-, 2971(24)-, 2980(25)-, 3100(26)-, 3220(16)-, and 3260(16)-keV states; and (3) the 2091(10)-, 2435(12)-, 2470(10) [tentative $4^+$]-, and 3073.6(3)-keV states for which there is no obvious reason they are not observed. Definite spins are not known for states in the last group, and nonobservation of these levels may indicate they have spins $J > 6$. States that merit special attention are discussed in detail in the following.

*1747.0-keV $0^+$ state.* This level is tentatively labeled as a $0^+$ state in Refs. [5,10,11,20]. It was not observed in reactor $(n,n'\gamma)$ [11] and $(\alpha,2n)$ [9] reactions. The state was observed in conversion electron measurements, but statistics prohibited a definite $J = 0$ assignment [21]. Two transitions are observed in this work that have angular distributions and excitation functions that confirm the $0^+$ spin and parity of this level. The excitation function for the 1182.9-keV transition is shown in Fig. 3 along with statistical model calculations supporting the $J = 0$ assignment.

*1752.6-keV $2^+$ state.* New transitions of 395.1 and 495.5 keV are assigned to this level. Both $\gamma$ rays have

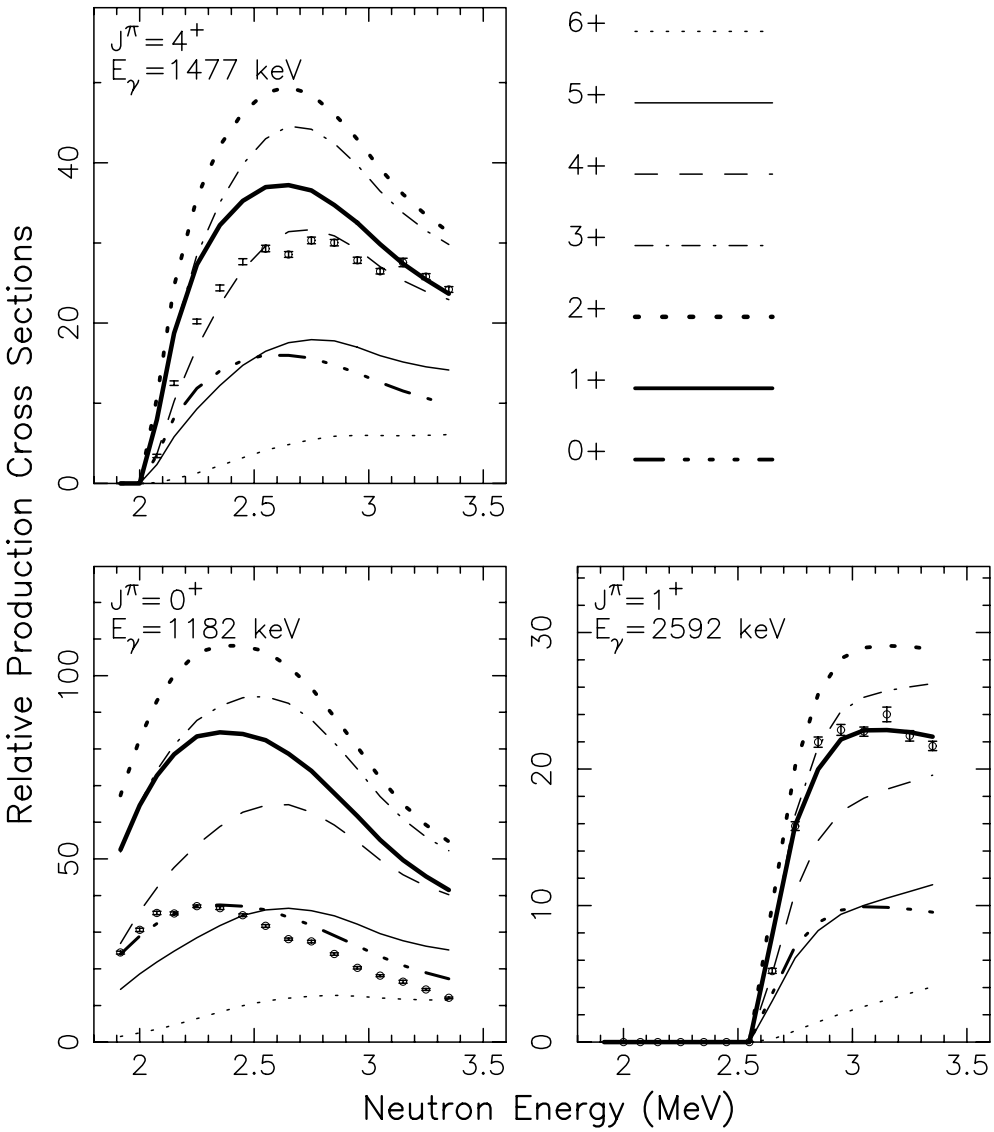


FIG. 3. $\gamma$-ray excitation functions compared to neutron production cross sections from statistical model calculations for transitions from states with spins of $J = 4^+$, $0^+$, and $1^+$. Such plots are used to confirm level spin assignments made from the angular distributions.

excitation functions that are consistent with those of the adopted 1188.5- and 1752.6-keV transitions, and both assignments are confirmed in the coincidence data. The mean lifetime of this level was determined to be $544^{+76}_{-64}$ fs from the Doppler shift of the 1188.5-keV transition at $E_n = 2.8$ MeV, as shown in Fig. 6(a). A similar $F(\tau)$ value was observed for the 1752.6-keV transition. The level has an adopted lifetime of $790 \pm 290$ fs [10], in agreement with our value. (The adopted value does have a compiler's note saying the matrix elements listed in the original paper [22] were interchanged and that the compiler switched values before calculating the half-life.) The branching ratios listed in Table I were determined using $A_0$ values from the $E_n = 2.8$ MeV angular distributions; consistent values were found using the excitation functions. The deduced transition rate $B(E2; 2^+_3 \rightarrow 0^+_2) = 194^{+26}_{-24}$ is uncommonly large for a nucleus considered to be vibrational. It is possible that strength is missing from unobserved decays to other low-lying levels; however, the branching ratio for the decay to the $0^+_2$ state would have to be lowered substantially for this transition rate to be unremarkable.

*1951.7-keV $3^+$ state.* No spin value was adopted in the compilation [10]. In work completed since the compilation, this level is assigned $J^\pi = 2^+$ [9] and $J^\pi = 3^+$ [5,11]. The angular distributions of our work support either assignment. There is a significant difference between the adopted branching ratios [10] and the values obtained in this work. Figure 4 shows a comparison between statistical model calculations and experimental excitation function data using branching ratios from this work and the adopted values. The new branching ratios consistently lead to a description of this state as $J = 3$ in comparisons between the relative $\gamma$-ray production cross sections and CINDY calculations, whereas the adopted branching ratios lead to different preferred $J$ values depending on the transition. All transitions from a level should line up with the same spin value in plots such as Fig. 4,

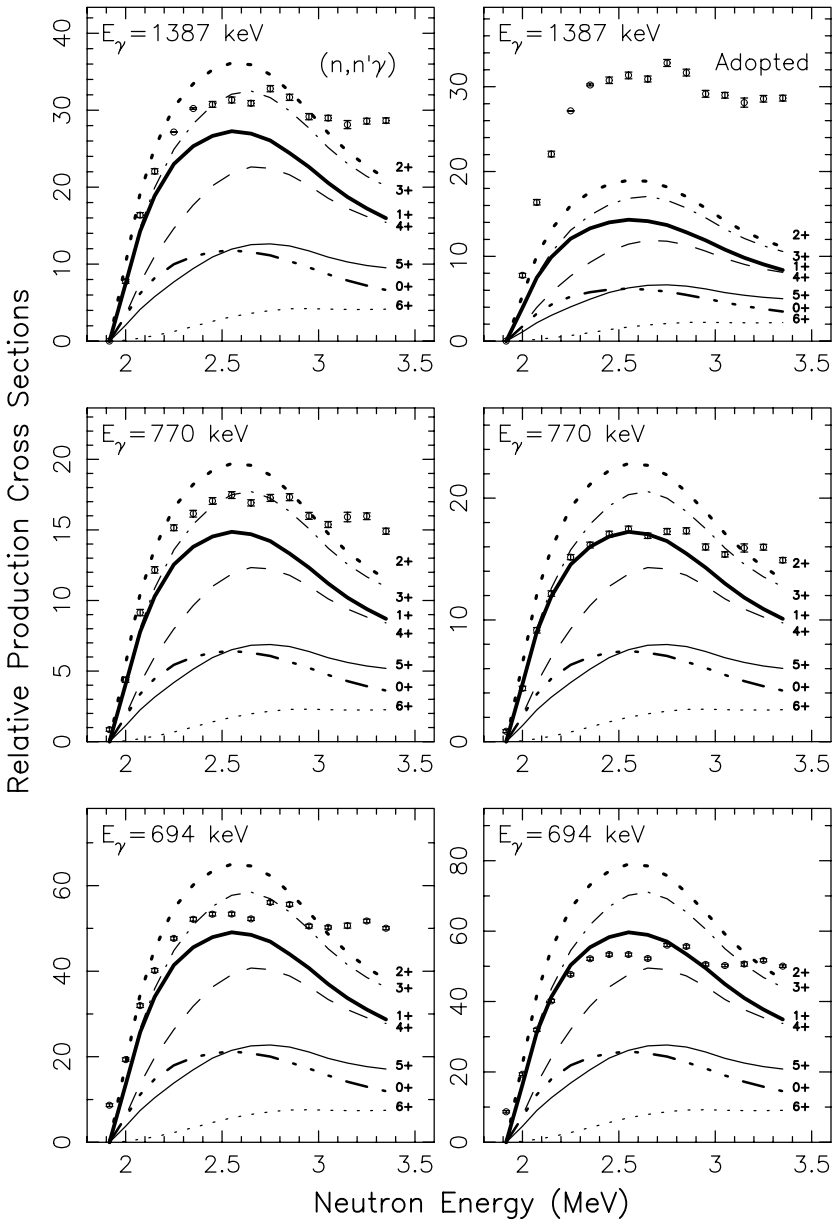


FIG. 4. $\gamma$-ray excitation functions compared to production cross sections from statistical model calculations for three transitions from the 1951.7-keV level. Branching ratios from this work were used in the left panels and adopted values were used for the comparisons on the right. Provided the branching ratios are correct all transitions from a level should align with the same $J$ value, as is observed for the $(n,n'\gamma)$ values in the left panels.

provided the branching ratios are correct. Missing strength from an unobserved transition could change our result, but the inconsistency observed with the adopted branching ratios [10] indicates a problem with those values. The combined information indicates the $J = 3$ assignment best describes this level.

*2310.7-keV state*. This state was previously assigned $J = 1$ based on a tentative $M1$ assignment for the 953-keV transition into the $0_2^+$ state [10]. The angular distribution of this transition in the current work has a distinctive $E2$ shape; additionally, the 1129.6-keV decay into the $4_1^+$ level is observed. The combined information leads to $J^\pi = 2^+$ for this level.

*2538.7-keV state*. This level is not adopted [10], but it is observed in reactor $(n,n'\gamma)$ [11] reactions and is assigned $J^\pi = 4^-$; it is also observed in $^{123}$Te$(d,t)^{122}$Te and $^{123}$Te($^3$He,$^4$He)$^{122}$Te reactions [5]. Our work supports the $J = 4$ assignment. The branching ratios observed in this work of (64:13:24) differ somewhat from the reactor $(n,n'\gamma)$ [11] values of (62:19:19) for the $4_1^- \rightarrow 3_1^+$, $4_1^- \rightarrow 4_2^+$, and $4_1^- \rightarrow 4_1^+$ transitions, respectively. The relative size of the branching ratios into the $4_1^+$ and $4_2^+$ states was used previously to support the argument that this state is predominantly a two-quasiparticle state [11].

*2592.5-keV state*. The adopted parity of this level is positive [10]. Schauer *et al*. [5] list the parity as negative and label this state as the $1^-$ member of the quadrupole-octupole phonon quintuplet. The parity question was not resolved by our work.

*2758.3-keV 6 and 2758.5-keV 5 states*. Four transitions are observed to decay from levels at 2758.3 and 2758.5 keV. The excitation functions support assigning the transitions of 351.2 and 1007.4 keV to the formerly adopted

TABLE I. Levels and transition rates in $^{122}$Te. Uncertainties are in the last digit(s). Transition rate uncertainties are from the uncertainties in the level lifetime and do not reflect uncertainties in the multipole-mixing ratio. The adopted energy of the $2_1^+$ state was used for level development. Horizontal lines indicate changes in the energy of the angular distribution used for extracting level information, and brackets indicate a tentative assignment. An $E1$ in the mixing ratio column indicates that a B($E1$) value is given in the B($M1$) column. The mixing ratios and B(XL)s presented are those of the first spin listed when the spin of the initial state is not definite.

| $J^\pi$ | $E_x$ (keV) | Note | $E_\gamma$ (keV) | $E_f$ (keV) | BR (%) | $\tan^{-1}(\delta)$ | $F(\tau)$ | $\tau$ (fs) | B($M1$) (W.u.) | B($E2$) (W.u.) |
|---|---|---|---|---|---|---|---|---|---|---|
| $2^+$ | 564.12(1) | a | 564.01(13) | 0 | 100 | | | $10700^{+70}_{-70^a}$ | | $37.2^{+2}_{-3}$ |
| $4^+$ | 1181.23(7) | a | 617.12(5) | 564 | 100 | | | | | |
| $2^+$ | 1256.83(4) | a | 692.66(5) | 564 | 83.1(2) | $-0.97^{+19}_{-19}$ | | | $2.2^{+10}_{-9}E$-2 | $71^{+33}_{-30}$ |
| | | a | 1256.87(5) | 0 | 16.9(2) | | 0.043(18) | $1140^{+840}_{-360}$ | | $1.07^{+46}_{-50}$ |
| $0^+$ | 1357.3(1) | a | 793.18(9) | 564 | 100 | | | >2 ps | | <36 |
| $0^+$ | 1746.99(7) | e | 490.06(20) | 1256 | 29.3(6) | | | | | <124 |
| | | | 1182.88(5) | 564 | 70.7(6) | | | >1.9 ps | | <4 |
| $6^+$ | 1750.91(9) | a | 569.68(5) | 1181 | 100 | | | | | |
| $2^+$ | 1752.60(5) | c | 395.07(21) | 1357 | 4.5(1) | | | | | $194^{+26}_{-24}$ |
| | | c | 495.54(22) | 1256 | 4.3(1) | $-0.50^{+16}_{-13}$ | | | $1.6^{+2}_{-2}E$-2 | $14^{+2}_{-2}$ |
| | | ac | 1188.48(5) | 564 | 31.2(2) | $1.22^{+16}_{-22}$ | | | $1.3^{+2}_{-2}E$-3 | $4.9^{+6}_{-6}$ |
| | | | | | | $-0.03^{+19}_{-19}$ | | | $1.1^{+1}_{-1}E$-2 | $5.0^{+1}_{-1}E$-3 |
| | | ac | 1752.64(6) | 0 | 60.0(2) | | 0.093(11) | $544^{+76}_{-64}$ | | $1.5^{+2}_{-2}$ |
| $4^+$ | 1909.50(5) | | 652.62(5) | 1256 | 13.4(3) | | | | | $21^{+6}_{-6}$ |
| | | a | 728.19(5) | 1181 | 49.6(3) | $1.35^{+3}_{-3}$ | | | $1.6^{+5}_{-5}E$-3 | $43^{+13}_{-12}$ |
| | | a | 1345.53(7) | 564 | 37.0(3) | | 0.043(12) | $1230^{+510}_{-280}$ | | $1.5^{+5}_{-5}$ |
| $0^+$ | 1940.01(7) | a | 683.10(6) | 1256 | 96.0(3) | | | | | <74 |
| | | a | 1376.02(9) | 564 | 4.0(3) | | | >2 ps | | <0.1 |
| $3^+$ | 1951.68(5) | ae | 694.87(10) | 1256 | 53.8(4) | $0.00^{+6}_{-3}$ | | | | |
| | | a | 770.07(5) | 1181 | 16.3(4) | $-0.22^{+19}_{-16}$ | | | | |
| | | a | 1387.79(5) | 564 | 29.9(3) | $-1.54^{+3}_{-3}$ | | | | |
| $4^+$ | 2041.07(6) | d | 783.66(31) | 1256 | 7.3(2) | | | | | $6.6^{+10}_{-10}$ |
| | | a | 859.70(5) | 1181 | 45.5(3) | $0.66^{+12}_{-19}$ | | | $1.7^{+2}_{-3}E$-2 | $9.7^{+15}_{-14}$ |
| | | a | 1477.07(5) | 564 | 47.2(3) | | 0.061(9) | $856^{+147}_{-116}$ | | $1.8^{+3}_{-3}$ |
| $2^+$ | 2099.22(6) | ak | 1535.11(6) | 564 | 96.4(2) | $1.16^{+3}_{-3}$ | | | $3.6^{+3}_{-3}E$-3 | $5.7^{+4}_{-4}$ |
| | | | | | | $0.00^{+6}_{-3}$ | | | $2.2^{+2}_{-2}E$-2 | 0 |
| | | k | 2098.88(35) | 0 | 3.6(2) | | 0.129(9) | $377^{+30}_{-27}$ | | $5.3^{+4}_{-4}E$-2 |
| $3^-$ | 2196.80(4) | | 939.92(6) | 1256 | 1.4(2) | $E1$ | | | $4.4^{+2}_{-2}E$-5 | |
| | | d | 1014.87(10) | 1181 | 3.1(2) | $E1$ | | | $7.7^{+3}_{-3}E$-5 | |
| | | | 1632.86(5) | 564 | 95.5(3) | $E1$ | 0.274(8) | $150^{+5}_{-5}$ | $5.7^{+2}_{-2}E$-4 | |
| 1 | 2203.75(5) | k | 946.77(12) | 1256 | 7.0(3) | $0.94^{+63}_{-66}$ | | | | |
| | | k | 1639.69(3) | 564 | 72.0(3) | $0.19^{+41}_{-38}$ | | | | |
| | | k | 2203.58(10) | 0 | 21.0(3) | | 0.237(10) | $182^{+10}_{-10}$ | | |
| $6^+$ | 2283.45(7) | a | 532.48(9) | 1751 | 51.9(22) | $0.19^{+37}_{-25}$ | | | $4.9^{+45}_{-33}E$-1 | $46^{+42}_{-30}$ |
| | | a | 1102.28(9) | 1181 | 48.1(22) | | 0.208(128) | $214^{+420}_{-102}$ | | $31^{+29}_{-21}$ |
| $2^+$ | 2287.36(5) | | [1030.18(15)] | 1256 | 5.0(1) | $-0.97^{+66}_{-69}$ | | | $2.2^{+2}_{-1}E$-3 | $3.1^{+2}_{-2}$ |
| | | | 1105.50(50) | 1181 | 2.0(1) | | | | | $1.3^{+1}_{-1}$ |
| | | a | 1723.23(5) | 564 | 84.2(4) | $0.91^{+9}_{-13}$ | | | $9.2^{+5}_{-5}E$-3 | $3.7^{+2}_{-2}$ |
| | | | | | | $0.31^{+13}_{-9}$ | | | $2.2^{+1}_{-1}E$-2 | $5.5^{+3}_{-3}E$-1 |
| | | a | 2287.52(15) | 0 | 8.8(3) | | 0.208(8) | $214^{+11}_{-11}$ | | $0.15^{+1}_{-1}$ |
| $0^+$ | 2297.46(6) | dk | 1733.34(6) | 564 | 100 | | 0.041(16) | $1290^{+870}_{-370}$ | | $1.1^{+5}_{-5}$ |
| $2^+$ | 2310.68(5) | c | 557.82(50) | 1752 | 4(3) | $-1.00^{+56}_{-57}$ | | | $1.7^{+5}_{-5}E$-3 | $9.7^{+26}_{-26}$ |
| | | a | 953.05(16) | 1357 | 3.9(1) | | | | | $9.1^{+25}_{-25}E$-1 |

TABLE I. (*Continued*.)

| $J^\pi$ | $E_x$ (keV) | Note | $E_\gamma$ (keV) | $E_f$ (keV) | BR (%) | $\tan^{-1}(\delta)$ | $F(\tau)$ | $\tau$ (fs) | B($M1$) (W.u.) | B($E2$) (W.u.) |
|---|---|---|---|---|---|---|---|---|---|---|
| | | a | 1129.64(24) | 1181 | 3.3(1) | | | | | $3.3^{+89}_{-89}E$-1 |
| | | a | 1746.59(6) | 564 | 88.8(4) | $-1.48^{+6}_{-3}$ | 0.043(11) | $1230^{+450}_{-260}$ | $3.5^{+10}_{-10}E$-5 | $1.0^{+3}_{-3}$ |
| | | | | | | $-0.50^{+6}_{-6}$ | | | $3.3^{+9}_{-9}E$-3 | $2.3^{+6}_{-6}E$-1 |
| $5^-$ | 2407.12(9) | a | 1225.89(9) | 1181 | 100 | $E1$ | 0.156(16) | $303^{+41}_{-32}$ | $7.0^{+9}_{-9}E$-4 | |
| $2^+$ | 2407.96(5) | ak | 1843.84(5) | 564 | 100 | $1.13^{+28}_{-41}$ | 0.293(12) | $137^{+8}_{-8}$ | $6.7^{+4}_{-4}E$-3 | $6.4^{+4}_{-4}$ |
| $(4^+)$ | 2448.47(5) | e | 1267.25(5) | 1181 | 91.6(8) | $0.09^{+12}_{-19}$ | | | $4.2^{+5}_{-6}E$-2 | $1.5^{+2}_{-2}E$-1 |
| | | | 1884.27(12) | 564 | 8.4(8) | | 0.141(17) | $341^{+51}_{-43}$ | | $2.4^{+3}_{-3}E$-1 |
| $0^+$ | 2499.59(8) | dgk | 1242.80(11) | 1256 | 22.2(8) | | | | | $1.6^{+9}_{-9}$ |
| | | k | 1935.43(11) | 564 | 77.6(8) | | 0.049(25) | $1080^{+1180}_{-380}$ | | $6.0^{+31}_{-33}E$-1 |
| $2^+$ | 2508.64(5) | k | 1251.64(30) | 1256 | 8.8(3) | $-0.19^{+44}_{-37}$ | | | $1.52^{+7}_{-7}E$-2 | $2.6^{+2}_{-2}E$-1 |
| | | ak | 1944.53(5) | 564 | 91.2(3) | $1.00^{+13}_{-9}$ | 0.387(11) | $91^{+4}_{-4}$ | $1.3^{+6}_{-6}E$-2 | $5.8^{+3}_{-2}$ |
| 5 | 2535.68(9) | k | 1354.45(9) | 1181 | 100 | $-0.79^{+15}_{-16}$ | 0.024(51) | >680 fs | $<9.4E$-3 | 4.2 |
| $4^-$ | 2538.58(4) | c,k | 586.82(5) | 1951 | 64.3(6) | $E1$ | | | $<1.2^{+1}_{-1}E$-3 | |
| | | k | 629.07(8) | 1908 | 12.7(8) | $E1$ | | | $<1.9^{+2}_{-2}E$-4 | |
| | | k | 1357.54(10) | 1181 | 23.0(6) | $E1$ | 0.017(29) | >1.1 ps | $<3.3^{+4}_{-3}E$-5 | |
| 2,3 | 2557.74(7) | k | 1300.91(7) | 1256 | 100 | $0.85^{+13}_{-12}$ | 0.117(9) | $421^{+41}_{-35}$ | | |
| $2^+$,3,4,5 | 2560.38(21) | d | 1379.15(21) | 1181 | 100 | | | | | |
| $1\pm$ | 2592.73(7) | ae | 1335.99(13) | 1256 | 9.4(8) | $0.94^{+314}_{-314}$ | | | $1.7^{+2}_{-2}E$-2 | $12.6^{+10}_{-9}$ |
| | | a | 2029.25(17) | 564 | 21.2(8) | $0.13^{+314}_{-314}$ | | | $3.0^{+3}_{-3}E$-2 | $9.1^{+8}_{-6}E$-2 |
| | | a | 2592.44(10) | 0 | 69.4(1) | | 0.693(12) | $26^{+2}_{-2}$ | $4.9^{+4}_{-4}E$-2 | |
| 3 | 2600.78(6) | ek | 1419.58(6) | 1181 | 67.2(1.1) | $1.10^{+19}_{-66}$ | | | | |
| | | k | 2036.57(12) | 564 | 32.8(1.1) | $-0.69^{+16}_{-15}$ | 0.049(30) | $1080^{+1790}_{-440}$ | | |
| 4 | 2603.74(14) | dgk | 1422.51(14) | 1181 | 100 | $0.66^{+15}_{-57}$ | | | | |
| (1,2,3) | 2636.01(5) | dgk | 1379.14(5) | 1256 | 84.4(7) | $(1.32^{+6}_{-9})$ | | | | |
| | | dgk | 2072.16(15) | 564 | 15.6(7) | $(-1.13^{+66}_{-38})$ | | | | |
| | 2637.85(40) | dv | 2073.73(36) | 564 | 100 | | | | | |
| 2,3 | 2654.39(6) | k | 1397.54(6) | 1256 | 82.6(7) | $-1.41^{+16}_{-6}$ | | | | |
| | | k | 2091.00(36) | 564 | 17.4(7) | $1.29^{+35}_{-38}$ | 0.073(34) | $708^{+660}_{-242}$ | | |
| $3^+$ | 2669.04(6) | k | 1487.80(7) | 1181 | 83.7(11) | $-0.09^{+9}_{-10}$ | | | $1.7^{+8}_{-7}E$-2 | $4.4^{+2}_{-2}E$-2 |
| | | k | 2104.96(15) | 564 | 16.3(11) | $-0.66^{+28}_{-34}$ | 0.103(40) | $484^{+339}_{-149}$ | $7.2^{+4}_{-3}E$-4 | $7.0^{+31}_{-29}E$-2 |
| $4^+$ | 2679.39(6) | dg | 1422.51(6) | 1256 | 29.6(15) | | | | | $1.9^{+6}_{-6}$ |
| | | | 2116.02(25) | 564 | 70.4(15) | | 0.085(24) | $599^{+257}_{-142}$ | | $6.3^{+20}_{-19}E$-1 |
| $4^+$ | 2693.57(6) | ek | 1436.59(39) | 1256 | 7.3(16) | | | | | $1.3^{+3}_{-3}$ |
| | | k | 1512.35(6) | 1181 | 92.7(16) | $0.06^{+85}_{-19}$ | 0.210(39) | $212^{+61}_{-41}$ | $4.0^{+10}_{-9}E$-2 | $4.5^{+1}_{-1}E$-2 |
| 1 | 2719.22(9) | ad | 2155.18(12) | 564 | 55.9(13) | $0.22^{+314}_{-314}$ | | | | |
| | | ak | 2719.14(12) | 0 | 44.1(13) | | 0.366(40) | $98^{+19}_{-15}$ | | |
| 1 | 2742.45(9) | | 1485.59(15) | 1256 | 15.4(4) | $-0.72^{+314}_{-314}$ | | | | |
| | | | 2178.35(11) | 564 | 84.6(4) | $0.81^{+138}_{-112}$ | 0.330(34) | $116^{+19}_{-16}$ | | |
| $0^+$ | 2755.68(8) | a | 1498.71(9) | 1256 | 53.8(6) | | | | | $7.8^{+16}_{-15}$ |
| | | a | 2192.46(22) | 564 | 46.2(6) | | 0.219(35) | $207^{+49}_{-35}$ | | $1.0^{+2}_{-2}$ |
| $6^-$ | 2758.48(6) | ac | 351.20(24) | 2407 | 67.3(11) | $-0.31^{+9}_{-7}$ | | | | |
| | | | 1007.39(12) | 1751 | 32.7(11) | $E1$ | | | | |
| $5\ (^+)$ | 2758.30(11) | c | 717.20(14) | 2040 | 18.0(5) | $1.26^{+16}_{-9}$ | | | $7.5^{+9}_{-9}E$-3 | $101^{+11}_{-11}$ |
| | | | 1577.31(7) | 1181 | 82.0(5) | $0.47^{+9}_{-7}$ | 0.232(20) | $193^{+24}_{-19}$ | $2.7^{+3}_{-4}E$-2 | $2.0^{+3}_{-3}$ |
| 4,3,5 | 2770.47(9) | k | 1589.24(9) | 1181 | 100 | | 0.181(39) | $262^{+88}_{-56}$ | | |
| $2^+$,3,4,5 | 2772.45(8) | k | 1591.22(9) | 1181 | 100 | | 0.168(47) | $288^{+131}_{-75}$ | | $7.7^{+27}_{-24}$ |
| 2,3 | 2777.53(4) | k | 2213.41(11) | 564 | 100 | $-0.03^{+9}_{-6}$ | 0.256(15) | $170^{+14}_{-13}$ | | |

TABLE I. (*Continued*.)

| $J^\pi$ | $E_x$ (keV) | Note | $E_\gamma$ (keV) | $E_f$ (keV) | BR (%) | $\tan^{-1}(\delta)$ | $F(\tau)$ | $\tau$ (fs) | B($M1$) (W.u.) | B($E2$) (W.u.) |
|---|---|---|---|---|---|---|---|---|---|---|
| 2,3,4 | 2789.72(9) | k | 2225.60(13) | 564 | 100 | | | | | |
| 2,3 | 2796.21(7) | k | 2232.10(12) | 564 | 100 | $0.00^{+9}_{-9}$ | 0.686(15) | $28^{+2}_{-2}$ | | |
| 3 | 2801.35(9) | ek | 604.10(17) | 2197 | 14.5(10) | $0.44^{+35}_{-28}$ | | | | |
| | | k | 1544.46(48) | 1256 | 11.7(11) | $-1.29^{+16}_{-9}$ | | | | |
| | | k | 2237.40(12) | 564 | 73.8(13) | $-0.03^{+6}_{-6}$ | 0.112(17) | $459^{+92}_{-70}$ | | |
| | [2807.7(1)] | vt | [899.28(5)] | 1909 | | | | | | |
| $4^+$,3 | 2809.99(7) | dg | 1628.81(7) | 1181 | 91.8(7) | $0.03^{+22}_{-12}$ | | | | |
| | | | 2245.51(19) | 564 | 8.2(7) | | | | | |
| 5,4 | 2816.69(7) | e | 907.06(10) | 1909 | 29.3(14) | $0.19^{+32}_{-28}$ | | | | |
| | | | 1635.61(9) | 1181 | 70.7(14) | $0.44^{+9}_{-6}$ | 0.060(33) | $903^{+1150}_{-340}$ | | |
| | 2822.7(3) | dv | 1641.5(3) | 1181 | | | | | | |
| | 2837.47(4) | dv | 1656.24(40) | 1181 | | | | | | |
| | [2839.1(5)] | vt | [899.1(5)] | 1940 | | | | | | |
| 3 | 2839.48(6) | gk | 1582.42(12) | 1256 | 23.8(7) | $-0.03^{+19}_{-19}$ | | | | |
| | | dgk | 1658.29(6) | 1181 | 19.0(22) | $1.04^{+13}_{-50}$ | | | | |
| | | k | 2275.78(30) | 564 | 57.2(17) | $-0.69^{+19}_{-12}$ | 0.297(23) | $139^{+15}_{-15}$ | | |
| 5 | 2860.48(6) | | 452.10(22) | 2407 | 36.7(6) | $0.35^{+22}_{-22}$ | | | | |
| | | | 1679.33(6) | 1181 | 63.3(6) | $0.03^{+6}_{-3}$ | 0.214(30) | $214^{+42}_{-33}$ | | |
| 3,2 | 2885.67(11) | dgk | 1628.81(50) | 1256 | 10.8(6) | $1.26^{+9}_{-13}$ | | | | |
| | | k | 2321.55(11) | 564 | 89.2(6) | $0.47^{+6}_{-7}$ | 0.449(14) | $73^{+4}_{-4}$ | | |
| | [2889.7(10)] | acv | [1138.8(10)] | 1751 | | | | | | |
| | 2897.47(30) | dv | 1640.64(30) | 1256 | | | | | | |
| $4^+$,3,2(1) | 2898.90(14) | dv | 1642.60(30) | 1256 | | | | | | |
| | | | 2334.63(16) | 564 | | | 0.167(48) | $290^{+138}_{-77}$ | | |
| 5(−),(4) | 2901.05(11) | | 1719.82(11) | 1181 | | $E1$ | 0.122(39) | $415^{+216}_{-113}$ | $1.9^{+7}_{-7}E$-4 | |
| $4^+$,5,6 | 2910.82(21) | | 1159.91(21) | 1750 | | | | | | |
| $2^+$ | 2911.19(10) | ec | 1654.32(27) | 1256 | 16.3(4) | $-0.35^{+19}_{-25}$ | | | $6.9^{+6}_{-5}E$-3 | $2.4^{+2}_{-2}E$-1 |
| | | ac | 2347.08(11) | 564 | 76.4(5) | $0.50^{+41}_{-25}$ | | | $9.8^{+8}_{-7}E$-3 | $3.8^{+4}_{-3}E$-1 |
| | | c | 2911.46(80) | 0 | 7.3(4) | | 0.286(17) | $147^{+11}_{-11}$ | | $5.4^{+4}_{-4}E$-2 |
| | 2913.06(24) | dv | 1656.31(40) | 1256 | | | | | | |
| | | dv | 1731.79(30) | 1181 | | | | | | |
| 1 | 2915.96(10) | k | 2351.96(13) | 564 | 51.0(5) | $-0.31^{+44}_{-13}$ | | | | |
| | | k | 2915.81(16) | 0 | 49.0(5) | | 0.755(22) | $20^{+2}_{-2}$ | | |
| 1 | 2919.31(13) | k | 2919.31(13) | 0 | | | 0.530(29) | $53^{+6}_{-6}$ | | |
| 3(2) | 2930.13(12) | k | 1673.22(14) | 1256 | 40.3(7) | $-1.35^{+6}_{-6}$ | | | | |
| | | k | 2366.11(15) | 564 | 59.7(7) | $-0.06^{+6}_{-10}$ | 0.185(27) | $254^{+53}_{-38}$ | | |
| 4,5 | 2930.65(7) | k | 733.42(8) | 2196 | 26(2) | $0.66^{+6}_{-3}$ | | | | |
| | | k | 1750.01(12) | 1181 | 74(2) | $0.75^{+9}_{-9}$ | 0.500(34) | $60^{+9}_{-7}$ | | |
| 3,2,4 | 2938.94(11) | k | 2374.82(11) | 564 | | | 0.533(15) | $53^{+3}_{-3}$ | | |
| | 2944.11(80) | dv | 1762.88(80) | 1181 | | | | | | |
| $4^+$,3 | 2958.01(10) | | 1701.48(47) | 1256 | 15.3(3) | | | | | $1.4^{+2}_{-2}$ |
| | | | 1776.78(11) | 1181 | 52.6(5) | $0.41^{+35}_{-35}$ | | | $1.5^{+2}_{-2}E$-2 | $6.3^{+5}_{-5}E$-1 |
| | | | 2393.79(26) | 564 | 32.1(5) | | 0.257(14) | $169^{+13}_{-12}$ | | $5.5^{+5}_{-4}E$-1 |
| $(2^+,1)$ | 2959.08(15) | k | 2959.08(15) | 0 | | | | | | |
| | 2961.36(21) | dv | 1780.13(21) | 1181 | | | | | | |
| 4 | 2975.64(13) | k | 778.61(13) | 2196 | | $-1.04^{+16}_{-9}$ | | | | |
| 1 | 2982.26(8) | k | 1725.30(9) | 1256 | 22.9(9) | $0.28^{+314}_{-314}$ | | | | |

TABLE I. (*Continued*.)

| $J^\pi$ | $E_x$ (keV) | Note | $E_\gamma$ (keV) | $E_f$ (keV) | BR (%) | $\tan^{-1}(\delta)$ | $F(\tau)$ | $\tau$ (fs) | B($M1$) (W.u.) | B($E2$) (W.u.) |
|---|---|---|---|---|---|---|---|---|---|---|
| | | k | 2418.13(31) | 564 | 15.3(5) | $0.94^{+314}_{-314}$ | | | | |
| | | k | 2982.54(13) | 0 | 61.8(9) | | 0.473(63) | $67^{+19}_{-15}$ | | |
| $4^+$ | 2993.54(8) | | 1736.18(30) | 1256 | 12.6(5) | | | | | $2.5^{+9}_{-9}E$-1 |
| | | | 1812.34(9) | 1181 | 70.0(6) | $1.51^{+16}_{-9}$ | | | $1.9^{+7}_{-7}E$-5 | $1.1^{+4}_{-4}$ |
| | | | 2429.49(22) | 564 | 17.4(4) | | 0.072(24) | $742^{+399}_{-199}$ | | $6.3^{+3}_{-3}E$-2 |
| 5(3) | 2995.41(29) | k | 1086.71(29) | 1908 | | $-1.22^{+22}_{-16}$ | 0.104(132) | $494^{+648}_{-305}$ | | |
| 3,4 | 2997.96(8) | k | 1816.73(9) | 1181 | | | | | | |
| | | kv | 2433.83(14) | 564 | | | 0.451(29) | $73^{+8}_{-8}$ | | |
| | 3009.54(14) | | 2445.40(14) | 564 | | | | | | |
| 3 | 3012.55(11) | k | 1831.28(12) | 1181 | 63.0(6) | $0.13^{+13}_{-9}$ | | | | |
| | | k | 2448.58(21) | 564 | 37.0(6) | $0.03^{+10}_{-12}$ | 0.626(27) | $36^{+4}_{-4}$ | | |
| $2^+$ | 3026.77(6) | k | 468.81(22) | 2557 | 25.3(6) | $0.06^{+41}_{-25}$ | | | $3.2^{+6}_{-6}E$-1 | $3.7^{+7}_{-7}$ |
| | | k | 1074.90(10) | 1951 | 17.6(4) | $0.03^{+22}_{-22}$ | | | $1.8^{+3}_{-3}E$-2 | $1.0^{+2}_{-2}E$-2 |
| | | k | 1770.05(9) | 1256 | 46.7(6) | $0.56^{+22}_{-18}$ | | | $7.9^{+2}_{-2}E$-3 | $7.1^{+12}_{-12}E$-1 |
| | | k | 2462.5(21) | 564 | 10.4(8) | $-0.60^{+60}_{-141}$ | | | $6.2^{+10}_{-10}E$-4 | $3.4^{+6}_{-6}E$-2 |
| | | ku | 3026.94(51) | 0 | <0.2 | | 0.192(26) | $244^{+48}_{-35}$ | | <7$E$-4 |
| $6^+$,5,4 | 3030.49(10) | | 1849.26(10) | 1181 | 100 | | 0.200(33) | $233^{+57}_{-41}$ | | $4.5^{+10}_{-9}$ |
| $2^+$ | 3037.04(7) | dk | 1780.08(9) | 1256 | 29.4(12) | $-1.32^{+94}_{-32}$ | | | | |
| | | k | 1856.32(16) | 1181 | 25.0(10) | | | | | |
| | | k | 2472.71(20) | 564 | 45.6(12) | $1.16^{+16}_{-13}$ | | | | |
| | | ku | 3036.74(54) | 0 | <0.2 | | | | | |
| $2^+$,3,4,5 | 3042.00(12) | k | 1860.77(12) | 1181 | | | 0.444(26) | $75^{+8}_{-7}$ | | |
| $2^+$ | 3044.40(12) | adv | 945.50(50) | 2098 | | | | | | |
| | | k | 1787.46(24) | 1256 | <21 | $-0.41^{+54}_{-164}$ | | | | |
| | | a | 2480.35(16) | 564 | <66 | $-0.28^{+31}_{-35}$ | | | <3.8$^{+16}_{-14}E$-3 | <8.3$^{+34}_{-31}E$-2 |
| | | a | 3043.74(54) | 0 | <13 | | 0.159(63) | $306^{+179}_{-89}$ | | <3.7$^{+15}_{-14}E$-2 |
| 3(2) | 3047.71(12) | | 1790.39(24) | 1256 | 13.4(7) | $-0.75^{+81}_{-75}$ | | | | |
| | | | 1865.97(25) | 1181 | 37.7(8) | $-1.57^{+28}_{-29}$ | | | | |
| | | | 2484.17(18) | 564 | 48.9(9) | $-1.38^{+19}_{-22}$ | 0.357(34) | $106^{+17}_{-14}$ | | |
| $0^+$,1,2 | 3052.03(18) | a | 1795.21(19) | 1256 | 57.9(12) | | | | | $8.1^{+26}_{-21}$ |
| | | a | 2487.74(72) | 564 | 42.1(12) | | 0.405(70) | $87^{+30}_{-21}$ | | $1.2^{+4}_{-2}$ |
| | 3057.2(19) | | 1875.9(19) | 1181 | | | | | | |
| $2^+$ | 3060.98(31) | | 2496.71(39) | 564 | 16.4(6) | $-0.03^{+314}_{-314}$ | | | $1.2^{+2}_{-2}E$-3 | 0.0 |
| | | | 3061.24(50) | 0 | 83.6(6) | | 0.172(17) | $280^{+34}_{-32}$ | | $2.5^{+4}_{-3}E$-1 |
| | [3068.7(4)] | | [2504.6(4)] | 564 | | | | | | |
| $5^-$,2,3 | 3069.37(9) | | 873.30(15) | 2195 | 11.4(7) | | | | | |
| | | | 1887.58(12) | 1181 | 88.6(7) | $1.44^{+6}_{-6}$ | 0.222(35) | $203^{+47}_{-34}$ | | |
| | 3071.15(16) | dg | 1890.03(18) | 1181 | 74.1(11) | | | | | |
| | | | 2506.46(41) | 564 | 25.9(11) | | | | | |
| $2^+$ | 3074.49(6) | dg | 1134.45(8) | 1940 | | | | | | |
| | 3080.7(14) | v | 1899.4(14) | 1181 | | | | | | |
| | 3084.5(13) | v | 1903.3(13) | 1181 | | | | | | |
| $5^+$ | 3086.20(8) | dg | 1134.45(8) | 1951 | 49.6(21) | | | | | |
| | | | 1905.46(72) | 1181 | 50.4(21) | | | | | |
| $2^+$ | 3094.60(6) | ct | 898.78(11) | 2195 | 18.7(6) | | | | | |

TABLE I. (*Continued*.)

| $J^\pi$ | $E_x$ (keV) | Note | $E_\gamma$ (keV) | $E_f$ (keV) | BR (%) | $\tan^{-1}(\delta)$ | $F(\tau)$ | $\tau$ (fs) | B($M1$) (W.u.) | B($E2$) (W.u.) |
|---|---|---|---|---|---|---|---|---|---|---|
| | | | 994.95(9) | 2099 | 31.4(6) | | | | | |
| | | | 1142.69(67) | 1951 | 9.4(8) | | | | | |
| | | | 1837.18(15) | 1256 | 28.2(6) | | | | | |
| | | | 2530.3(12) | 564 | 5.6(5) | | | | | |
| | | | 3093.99(51) | 0 | 6.7(4) | | | | | |
| 1,2 | 3104.13(52) | | 3104.13(52) | 0 | | | 0.231(106) | $194^{+208}_{-78}$ | | |
| 3 | 3112.67(19) | | 1161.36(26) | 1951 | 45.2(1) | $0.31^{+101}_{-71}$ | | | | |
| | | | 2548.15(26) | 564 | 54.8(1) | $-0.63^{+25}_{-28}$ | 0.050(52) | <1090 | | |
| $4^+$,2,3 | 3132.20(8) | | 935.57(16) | 2195 | 32.8(9) | $E1$ | | | $2.1^{+14}_{-13}E$-4 | |
| | | gtv | 1950.83(11) | 1181 | 14.4(13) | | | | | |
| | | | 2568.09(20) | 564 | 52.8(11) | | 0.071(43) | $753^{+1222}_{-303}$ | | $1.4^{+10}_{-9}E$-1 |
| | 3134.47(50) | gtv | 1953.24(50) | 1181 | 100 | | | | | |
| | 3139.14(14) | dg | 1958.31(14) | 1181 | 100 | | | | | |
| | 3142.8(5) | dg | 1961.61(50) | 1181 | 100 | | | | | |
| 3,1,2 | 3147.51(12) | | 1048.72(39) | 2099 | 20.0(13) | | | | | |
| | | dgv | 1890.27(15) | 1256 | 34.7(13) | | | | | |
| | | dgv | 2584.17(22) | 564 | 45.3(12) | | | | | |
| $0^+$,1,2 | 3150.67(22) | adgv | 2586.55(22) | 564 | | | 0.621(19) | $37^{+3}_{-3}$ | | $5.3^{+5}_{-4}$ |
| | 3153.15(22) | tv | 2589.03(22) | 564 | | | | | | |
| | 3155.82(22) | tv | 2591.70(22) | 564 | | | | | | |
| | 3157.81(11) | tv | 1900.98(11) | 1256 | | | | | | |
| 3 | 3159.76(13) | tv | 1903.0(13) | 1256 | | | | | | |
| | | | 1977.82(39) | 1181 | | | | | | |
| | | v | 2595.73(14) | 564 | | | | | | |
| | 3160.08(11) | v | 1903.25(11) | 1181 | | | | | | |
| | 3172.30(11) | dv | 1991.07(11) | 1181 | 84.2(19) | | | | | |
| | | | 2607.8(12) | 564 | 15.8(19) | | | | | |
| | 3177.13(7) | | 1077.88(8) | 2099 | | | | | | |
| | | v | 1920.50(21) | 1256 | | | | | | |
| 4,5,6 | 3183.10(37) | | 2001.87(37) | 1181 | | | 0.329(41) | $120^{+25}_{-19}$ | | |
| (5) | 3192.6(10) | | 2011.40(10) | 1181 | | $-0.66^{+50}_{-53}$ | 0.292(133) | $143^{+163}_{-63}$ | | |
| (5) | 3196.67(59) | | 2015.44(59) | 1181 | | $-0.66^{+35}_{-31}$ | | | | |
| 3(2,1) | 3198.22(15) | | 2634.10(15) | 564 | | $0.00^{+3}_{-3}$ | 0.423(28) | $81^{+10}_{-8}$ | | |
| 1 | 3199.34(55) | | 3199.34(55) | 0 | | | 0.612(49) | $38^{+8}_{-7}$ | | |
| 1 | 3207.76(19) | dg | 1950.91(21) | 1256 | 37.0(11) | | | | | |
| | | | 3207.88(52) | 0 | 63.0(11) | | 0.726(35) | $23^{+4}_{-4}$ | | |
| $0^+$,1,2,3 | 3209.88(12) | | 2645.76(16) | 564 | | | 0.886(35) | $8^{+3}_{-3}$ | | $22^{+13}_{-6}$ |
| | 3210.22(12) | d | 1300.65(17) | 1909 | | | | | | |
| | | d | 2029.12(17) | 1181 | | | | | | |
| | 3211.29(36) | dv | 1954.22(50) | 1256 | 43.1(15) | | | | | |
| | | | 2647.42(51) | 564 | 56.9(15) | | 0.507(79) | $58^{+21}_{-16}$ | | |
| $4^+$ | 3223.24(8) | | 1966.39(9) | 1256 | 26.4(9) | | | | | $2.1^{+3}_{-3}$ |
| | | | 2659.17(16) | 564 | 73.6(9) | | 0.377(30) | $98^{+14}_{-11}$ | | $1.3^{+2}_{-2}$ |
| | 3246.37(48) | dg | 1989.64(50) | 1256 | 74.4(12) | | | | | |
| | | | 2681.4(15) | 564 | 25.6(12) | | 0.276(105) | $153^{+129}_{-57}$ | | |
| 1(2) | 3252.50(15) | | 2688.40(16) | 564 | 55.8(14) | | | | | |
| | | | 3252.18(88) | 0 | 44.2(14) | | 0.414(91) | $84^{+39}_{-25}$ | | |
| | 3256.02(40) | dv | 2074.79(36) | 1181 | | | | | | |

TABLE I. (*Continued*.)

| $J^\pi$ | $E_x$ (keV) | Note | $E_\gamma$ (keV) | $E_f$ (keV) | BR (%) | $\tan^{-1}(\delta)$ | $F(\tau)$ | $\tau$ (fs) | B($M1$) (W.u.) | B($E2$) (W.u.) |
|---|---|---|---|---|---|---|---|---|---|---|
| | 3262.40(22) | | 2081.17(22) | 1181 | | | | | | |
| 1,2,3 | 3283.83(16) | | 2027.45(23) | 1256 | | | | | | |
| | | d | 2719.30(22) | 564 | | | | | | |
| 1 | 3289.10(54) | | 3289.10(54) | 0 | | | | | | |
| | 3293.22(51) | v | 2112.09(51) | 1181 | | | 0.726(72) | $23^{+9}_{-8}$ | | |
| | 3297.12(91) | v | 2733.00(90) | 564 | | | | | | |
| | 3300.73(50) | v | 1013.53(50) | 2287 | | | | | | |
| | 3302.62(36) | v | 2045.5(5) | 1256 | | | | | | |
| | | av | 2738.8(5) | 564 | | | | | | |
| | 3315.28(51) | v | 2751.2(5) | 564 | | | | | | |
| | 3333.51(51) | v | 2152.3(5) | 1181 | | | | | | |
| | 3335.73(51) | v | 2771.6(5) | 564 | | | | | | |
| | 3339.13(51) | v | 2775.0(5) | 564 | | | | | | |
| | 3357.13(51) | v | 2175.9(5) | 1181 | | | | | | |

[a]Adopted transition.
[c]See individual level discussion for this level.
[d]Doublet.
[e]Branching ratios from excitation functions.
[k]Calculations show strength is probably missing from this level.
[g]Doublet strength split using coincidence yields.
[t]Triplet transition.
[u]Observed in summed angle data only.
[v]Assignment based on coincidence data only.

level at 2758 keV with $J = 4^-, 5^-, 6^-$ [10]. Lee *et al*. [9] assign a 351-keV transition to a $6^-$ state at this energy. Transitions of 717.2 and 1577.3 keV are assigned to a new level at 2758.5 keV with $J = 5$ and a tentative positive parity. Angular momentum considerations and CINDY calculations exclude all of these transitions from belonging to the same level.

*2890.61-keV $5^+$,$6^+$,$7^+$ state*. An 1139.4-keV transition is adopted for this level [10]. A background line is observed. near 1139 keV that prohibits a definite assignment in our work, although we can say the transition is extremely weak if excited. A small line of the appropriate energy is observed in the coincidence data; therefore, the level and transition are listed as tentative in this work.

*2911.28-keV $2^+$ state*. A 2346.9-keV transition is adopted for this level [10]. We see two additional transitions of 1654.3 and 2911.5 keV, as well as a transition of 2347.1 keV. Each of these transitions is consistent with a $J = 2$ spin assignment. The ground-state transition is observed only at back angles where it is Doppler shifted away from the stronger 2914- and 2916-keV lines. The 2911.5-keV transition appears to have a very large Doppler shift relative to the other transitions assigned to this level, but it is only observed at a few angles. Two different Doppler shifts would indicate the level is a doublet, but the complex nature of the $\gamma$-ray energy region prohibits a doublet assignment. The lifetime listed in the table is due only to the 2347.1-keV Doppler shift.

*3044.3-keV $2^+$ state*. This adopted level has a 945.8-keV transition assigned to it with a 25% branch [10]. We see a 946.8-keV line, but most of its strength is assigned to the 2203.7-keV level. A weak 945-keV transition is observed in the 1535-keV coincidence gate, which indicates that the transition also belongs to this level. The branching ratio for the 945-keV transition cannot be determined, but these data indicate that it is significantly less than 25%.

## IV. MODEL DISCUSSION

### A. Overview

In the following sections we compare the structures and transitions observed in $^{122}$Te with model calculations using the IBM-2 with intruder-state mixing, the U(5) limit of the IBM-1, and the PCM. Calculated transition rates are presented in Table II for each of these models along with experimental values. The table is divided into an emerging normal and intruder band structure based on the IBM-2 calculations with intruder-state mixing.

### B. IBM-2 with intruder-state mixing

Intruder states from proton excitations across the $Z = 50$ closed shell have been observed rather convincingly in many nuclei near $Z = 50$, such as Cd [23,24], Sn [25,26], Sb [25], and I [27]. For the Te nuclei, such structures have remained

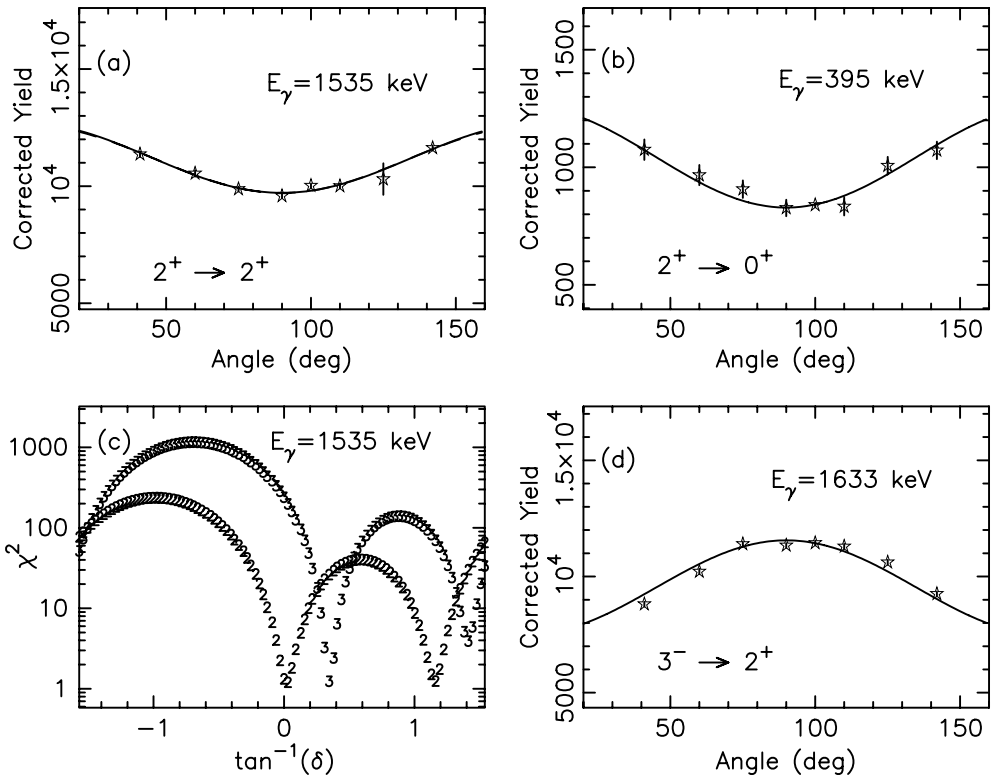


FIG. 5. (a) The $\gamma$-ray angular distribution along with a Legendre polynomial fit to the data for the 1535.1-keV transition from the 2099.2-keV level to the $2_1^+$ state. (c) The $\chi^2$ vs $\tan^{-1}\delta$ curve used to obtain the multipole-mixing ratio for the 1535.1-keV transition is shown. The number observed on each curve is the spin of the initial state. From this curve one cannot distinguish $J=2$ or $J=3$ as the spin of the level, although an observed ground-state transition unambiguously determines $J=2$ as the level spin. Two solutions for the multipole-mixing ratio for spin $J=2$ are determined from the curve. $\gamma$-ray angular distributions for transitions from the 1752.6-keV ($J=2$) level and the 2196.9-keV ($J=3$) level are shown in panels (b) and (d).

elusive and have mainly been identified only at high spins where band structures are evident [28,29]. Both the $0_2^+$ and $2_3^+$ states are predicted to have rather large intruder components in IBM-2 calculations and have been considered the lowest intruder states in $^{122}$Te [4,5,11,21,30]. Intruder bands built on such states have been suggested in calculations [4], but the level structure, decay characteristics, and transition rates between suggested band members have not been well enough established to test the predictions of the model.

The most comprehensive theoretical study of the Te isotopic chain was performed by Rikovska *et al.* [4] using the IBM-2, both with and without intruder-state mixing. Only the calculations with intruder-state mixing produced enough low-lying states to agree with the experimental data. We repeated those calculations for comparison with new data using model parameters obtained from the text and figures of Ref. [4] and the code NPBOS [31].

Within the framework of the IBM, the $^{122}$Te nucleus has two protons beyond the $Z=50$ shell and 12 neutron holes relative to $N=82$, or $N_\pi=1$ and $N_\nu=6$, respectively. A standard application of the IBM-2 [31] utilizes the Hamiltonian

$$H=\epsilon(n_\pi+n_\nu)+(V_{\pi\pi}+V_{\nu\nu})+\kappa Q_\pi\cdot Q_\nu+M_{\nu\nu}, \qquad (1)$$

where the terms represent the total d-boson energy, the anharmonicity due to like boson-boson interactions, the quadrupole-quadrupole interaction between neutron and proton bosons, and the Majorana symmetry term, respectively.

Intruder configurations are investigated within the framework of this model by treating the intruder 4p-2h states as contributing an extra pair of proton bosons, or with $N_\pi=3$ and $N_\nu=6$ for $^{122}$Te. Wave functions from the two configurations, normal and intruder, are then mixed together using the mixing operator [4,32]

$$H_{\rm mix}=\alpha\left(s_\pi^\dagger s_\pi^\dagger+s_\pi s_\pi\right)^{(0)}+\beta\left(d_\pi^\dagger d_\pi^\dagger+\tilde{d}_\pi\tilde{d}_\pi\right)^{(0)}, \qquad (2)$$

where $\alpha$ and $\beta$ are adjustable parameters describing the mixing between the two configurations. Further details of the calculational procedure for both energies and transition rates can be found in Ref. [4]. Parameters used in our calculations are given in Table III and were taken from the figures and the text of Ref. [4]. Transition rate parameters were varied slightly from those of Ref. [4] to reproduce the experimental B($E2$; $2_1^+\rightarrow 0_1^+$).

Level energies from these calculations are shown in the top panel of Fig. 7 and B($E2$) values are given in Table II in the column labeled IBM-2(MX). The level energies are plotted in emerging bands with levels having large intruder configurations in separate bands. The numbers in parentheses are the intruder percentages. The model does an excellent job of reproducing the number of low-lying positive parity states,

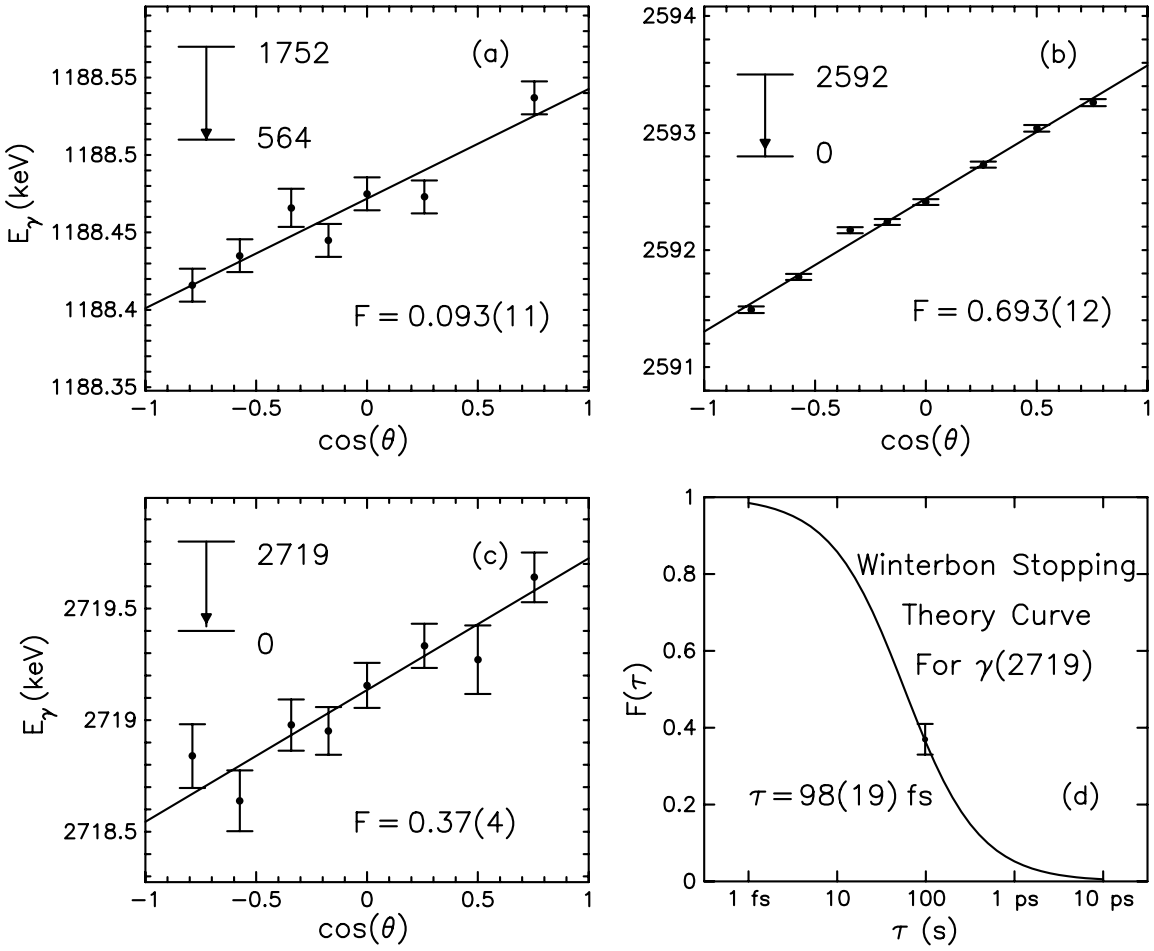


FIG. 6. Doppler shifts data for the (a) 1188.5-, (b) 2592.4-, and (c) 2719.2-keV transitions. (d) The Winterbon stopping theory calculations used to deduce $\tau$ from the Doppler shift of the 2719.2-keV transition shown in panel (c).

especially the extra $0^+$ states. In the second intruder band, the calculated $4^+$ state occurs above 3 MeV and is not shown in the figure. The model does not lead to the correct staggering of the levels in the quasi-$\gamma$ band, a characteristic that does appear in both U(5) and PCM calculations discussed later. This staggering occurs to some degree in $^{114-130}$Te and is possibly from interactions between normal excitations and intruder $4^+$ levels or two-quasiparticle admixtures [8].

Model B($E2$) values are compared to experimental values in the column labeled *with intruders* and are found to be in excellent agreement with the experimental data for many decays. Most notably the $2_3^+ \rightarrow 0_2^+$ transition is observed for the first time in this work. The observed B($E2$; $2_3^+ \rightarrow 0_2^+$) $= 194^{+26}_{-24}$ W.u. is unusually large for a vibrational nucleus, as previously discussed. The IBM-2 with intruder-state mixing calculations indicate that these two states, the $2_3^+$ and $0_2^+$ levels, are part of an emerging intruder band. Intruder orbitals are more deformed, and rotational bands built on intruder $0^+$ states are predicted to have large in-band transitions [21]. The IBM-2 calculations predict B($E2$) = 36 W.u. for this transition, as shown in Table II.

Collective intruder structures in $^{122}$Te might be expected to exhibit behavior analogous to that observed in the ground-state bands of deformed nuclei having the same number of valence particles as $^{122}$Te intruder levels and with the same neutron number [23], that is, $^{126}$Ba or $^{114}$Ru. The observed B($E2$; $2_1^+ \rightarrow 0_1^+$) for $^{126}$Ba is about 100 W.u. [33]; the $^{114}$Ru value has not been measured. The B($E2$; $2_1^+ \rightarrow 0_1^+$) observed for $^{126}$Ba is consistent with the large value observed in $^{122}$Te. This comparison supports the interpretation of the $0_2^+$ state as the band head for an intruder band in $^{122}$Te. The systematics of this level across the chain of Te isotopes also supports its identification as an intruder level. The energy of the $0_2^+$ level is lowest at midshell, where the number of $n$-$p$ interactions is maximized, and it follows a parabolic trajectory of increasing energy as the $N = 82$ shell is approached. The $2^+$ member of this band should be characterized by a small positive $\delta$ [34]. Our value of $\delta = -0.03 \pm 0.19$ is consistent with this expectation.

### C. Vibrational limit [U(5)]

The U(5) symmetry of the IBM-1 may be used to identify multiphonon structures in nuclei. $^{122}$Te has been investigated previously in Refs. [2,4,5] with this model. We have repeated

TABLE II. Comparisons of B($E2$) values with model calculations. Comparisons are separated into bands as displayed in Figs. 7 and 8. All values are in Weisskopf units (W.u. = 0.00359 $e^2b^2$ for $E2$ transitions.) The band labels $N$ and $I$ refer to normal and intruder bands, respectively, as determined from the IBM-2(MX) calculations.

| | Transition sequence | U(5) | Expt.[a] w/o intruders | PCM | | | IBM-2(MX) Rikovska[c] | Prior expt. | Expt.[b] with intruders |
|---|---|---|---|---|---|---|---|---|---|
| | | | | SP-Warr(1) | SP-Warr(2) | SP-Kisslinger | | | |
| $N_1$ band | $2_1^+ \to 0_1^+$ | 37.2 | | 37.1 | 37.1 | 37.1 | 36.9 | 37.2(2)[c] | |
| | $4_1^+ \to 2_1^+$ | 64.7 | | 46.5 | 45.1 | 46.4 | 57.8 | | |
| | $6_1^+ \to 4_1^+$ | 80.3 | | 31.2 | 33.6 | 30.1 | 68.9 | | |
| $N_2$ band | $0_2^+ \to 2_1^+$ | 59.7 | 36 | 4.4 | 1.1 | 3.7 | 1.3 | | <36 |
| | $2_2^+ \to 0_1^+$ | 0.6 | 1.07(50) | 0.05 | 0.3 | 0.1 | 0.5 | 1.17(28)[c] | 1.07(50) |
| | $2_2^+ \to 2_1^+$ | 39.8 | 71(33) | 35.3 | 26.8 | 22.1 | 53.3 | 97.5[d] | 71(33) |
| | $4_2^+ \to 2_1^+$ | 0.7 | 1.5(5) | 0.007 | 0.1 | 0.2 | 0.06 | | 1.5(5) |
| | $4_2^+ \to 4_1^+$ | 19.3 | 43(13) | 7.0 | 5.7 | 1.9 | 30.0 | | 43(13) |
| | $4_2^+ \to 2_2^+$ | 31.3 | 21(6) | 18.2 | 20.1 | 21.6 | 36.1 | | 21(6) |
| | $5_1^+ \to 4_1^+$ | 0.8 | <4.2 | 1.0 | 1.6 | 0.06 | 1.4 | | <4.2 |
| | $6_2^+ \to 4_1^+$ | 0.6 | 31(29) | 1.9 | 2.7 | 1.9 | 0.0 | | 31(29) |
| | $6_2^+ \to 6_1^+$ | 11.5 | 46(42) | 2.0 | 1.9 | 0.4 | 20.2 | | 46(42) |
| $I_1$ band | $2_3^+ \to 0_1^+$ | 0.0 | 0.053(4) | 0.7 | 1.5 | 0.3 | 0.03 | | 1.5(2) |
| | $2_3^+ \to 0_2^+$ | 33.4 | | 2.4 | 1.9 | 4.3 | 36.5 | | 194(26) |
| | $2_3^+ \to 2_2^+$ | 13.1 | | 0.06 | 0.03 | 0.1 | 5.2 | | 14(2) |
| | $2_3^+ \to 2_1^+$ | 0.6 | 5.7(4) | 8.2 | 8.2 | 20.6 | 0.0 | | 4.9(6) |
| | $4_3^+ \to 2_1^+$ | 0.00 | 0.24(3) | 8.4 | 9.1 | 9.0 | 0.03 | | 1.8(3) |
| | $4_3^+ \to 4_1^+$ | 0.1 | 0.15(2) | 8.1 | 7.3 | 9.4 | 0.03 | | 0.11(2) |
| | $4_3^+ \to 2_2^+$ | 0.9 | | 2.2 | 1.9 | 1.8 | 0.00 | | 6.6(10) |
| $I_2$ band | $0_3^+ \to 2_2^+$ | 20.9 | <74 | 22.5 | 22.1 | 13.0 | 0.6 | | <140 |
| | $0_3^+ \to 2_1^+$ | 0.2 | <0.1 | 14.4 | 12.0 | 18.4 | 0.2 | | <4 |
| | $2_4^+ \to 2_1^+$ | 0.0 | 3.7(2) | 0.07 | 0.03 | 0.06 | 0.0 | | 5.7(4) |
| | $2_4^+ \to 0_1^+$ | 0.0 | 0.15(1) | 0.1 | 0.9 | 0.008 | 0.0 | | 0.053(4) |
| $N_3$ band | $0_4^+ \to 2_2^+$ | 0.8 | | 27.4 | 18.1 | 26.2 | 1.8 | | <74 |
| | $0_4^+ \to 2_1^+$ | 0.0 | 1.1(5) | 0.0007 | 0.56 | 0.03 | 0.006 | | <0.1 |
| | $2_5^+ \to 2_2^+$ | 0.06 | | 1.4 | 1.6 | 0.6 | 0.7 | | 3.1(2) |
| | $2_5^+ \to 4_1^+$ | 0.1 | 0.33(89) | 0.2 | 0.4 | 3.2 | 0.06 | | 1.3(1) |
| | $2_5^+ \to 2_1^+$ | 0.0 | 1.0(3) | 0.4 | 0.9 | 0.1 | 0.0 | | 3.7(2) |
| | $2_5^+ \to 0_1^+$ | 0.0 | | 0.03 | 0.004 | 0.1 | 0.0 | | 1.3(1) |
| | $4_4^+ \to 4_1^+$ | 0.6 | | 3.6 | 2.3 | 0.1 | 0.08 | | 0.15(2) |
| | $4_4^+ \to 2_1^+$ | 0.0 | | 1.4 | 2.1 | 0.3 | 0.0 | | 0.24(3) |

[a]States with 50% intruder configurations in the IBM-2(MX) calculations are removed from level ordering.
[b]Levels are ordered as they appear experimentally.
[c]Ref. [4].
[d]Ref. [6] and references therein.

TABLE III. Model parameters used in IBM-2 calculations.

| | $\epsilon$ (MeV) | $\kappa$ (MeV) | $\chi_\pi$ | $\chi_\nu$ | $\xi_1$ | $\xi_2$ | $\xi_3$ | $e_\pi$ ($e$) | $e_\nu$ ($e$) | $C_{0\nu}$ (MeV) | $C_{2\nu}$ (MeV) | $C_{4\nu}$ (MeV) | $\alpha$ (MeV) | $\beta$ (MeV) | $\Delta$ (MeV) | $e_3/e_1$ |
|---|---|---|---|---|---|---|---|---|---|---|---|---|---|---|---|---|
| Normal | 0.860 | −0.160 | −1.000 | 0.250 | 0.20 | 0.10 | 0.20 | 0.14 | 0.12 | 0.040 | −0.124 | −0.100 | | | | |
| Intruder | 0.600 | −0.241 | −1.200 | 0.250 | 0.20 | 0.10 | 0.20 | 0.14 | 0.12 | 0.040 | −0.124 | −0.100 | 0.19 | 0.095 | 5.18 | 0.128 |

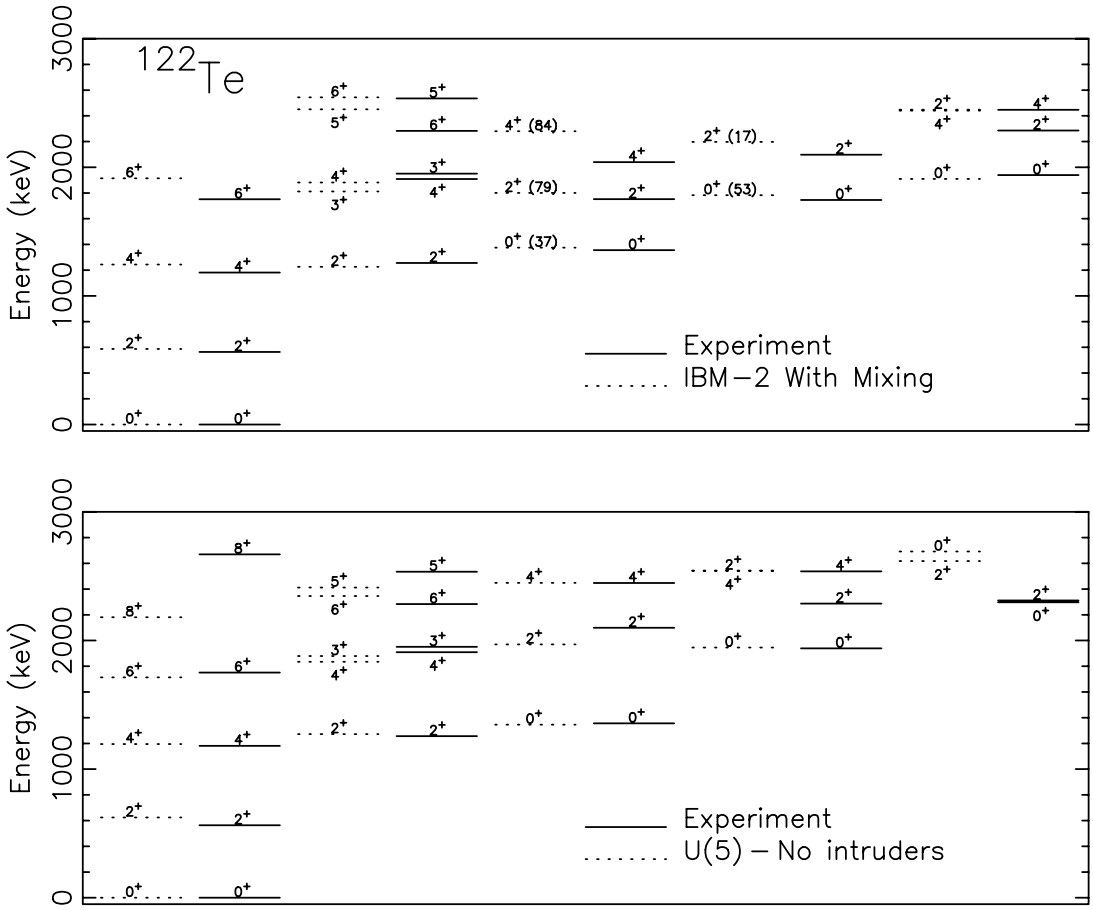


FIG. 7. (Top panel) IBM-2 with intruder-state mixing calculations compared with experimental levels. The levels are divided into normal and intruder bands based on the percentage of intruder configurations in the IBM-2 wavefunctions. The intruder percentages are given in parentheses. (Bottom panel) Comparison of U(5) level energies with experiments. All states with intruder configurations greater than 50% in the top panel are removed from the comparison in the bottom panel.

the U(5) calculations for comparison with our new data. The expression used to calculate the U(5) energies is

$$E(U5) = \epsilon n_d + \alpha n_d(n_d + 4) + \beta v(v + 3) + \gamma I(I + 1), \quad (3)$$

where $n_d$ and $v$ are the number of d bosons and d-boson seniority, respectively, and $\alpha$, $\beta$, $\gamma$, and $\varepsilon$ are adjustable parameters. Several previous authors have investigated $^{122}$Te and determined parameters to best describe this nucleus. Parameter sets from Refs. [2,5,35] were used in this investigation, which was extended to include four phonon structures. The parameter sets used are listed in Table IV. Experimental results and U(5) calculations were compared by first removing any level with a greater than 50% intruder contribution as determined from the IBM-2 calculations previously discussed. This procedure was used previously [2,4,5,29], and in each case the authors noted that the remaining low-lying levels appear to be well described by the model. Although the parameter sets determined in Refs. [5,29] best describe the suggested 1-, 2-, and 3-phonon states, when the 4-phonon levels are included, the parameters of Ref. [2] give the smallest average deviation for all states.

TABLE IV. Model parameters used in U(5) calculations.

| Source | $\epsilon$ (keV) | $\alpha$ (keV) | $\beta$ (keV) | $\gamma$ (keV) |
|---|---|---|---|---|
| Ref. [2] | 672.7 | 0 | −4.1 | −5.5 |
| Refs. [5,35] | 468.70 | 35.9 | −9.9 | −4.9 |

In Fig. 7 the U(5) calculated energies are shown along with the experimental levels. This model does reproduce the staggering observed in the second band; in fact, the correct order is observed for almost all of the levels considered. The model does an excellent job of reproducing the level energies once the states with large intruder configurations are removed. Reduced transition probabilities from the U(5) calculations are listed in Table II along with the experimental rates for the corresponding levels. The calculated B($E2$) values for the $0^+_{3,4}$, $2^+_{3,4,5}$, and $4^+_{3,4}$ levels are compared to the those from the experimental $0^+_{4,5}$, $2^+_{4,5,6}$, and $4^+_{4,5}$ states in the experimental data column labeled *w/o intruders*. The U(5) transition rate calculations were made using PHINT [36] with parameters reduced from the IBM-2 normal parameters from Ref. [4],

TABLE V. Model parameters used in PCM calculations.

| Source/Ref. | Orbital energies (keV) | | | | | Pairing G | Phonon energies (keV) | | Couplings | | $e_{\rm eff}$ ($e$) | $C_2$ (MeV) | $C_3$ (MeV) |
|---|---|---|---|---|---|---|---|---|---|---|---|---|---|
| | $g_{7/2}$ | $d_{5/2}$ | $h_{11/2}$ | $d_{3/2}$ | $s_{1/2}$ | | $\hbar\omega_2$ | $\hbar\omega_3$ | $\xi_2$ | $\xi_3$ | | | |
| Warr(1) [40] | 0 | 1000 | 2030 | 3190 | 3300 | 0.17 | 1171 | 1600 | 2.60 | 2.42 | 1.58 | 253 | 298 |
| Warr(2) [40] | 0 | 1000 | 2030 | 3190 | 3300 | 0.16 | 1171 | 1400 | 3.00 | 2.76 | 1.00 | 189 | 261 |
| Kisslinger [42] | 0 | 520 | 2030 | 3190 | 3300 | 0.18 | 1171 | 1800 | 2.60 | 2.15 | 1.61 | 253 | 335 |

and with E2DD $= -0.62$ $e$ b and E2SD $= 0.105$ $e$ b. These rates agree very well with many of the observed values. It appears that $^{122}$Te is much more like its Cd mirror than was previously thought.

### D. Particle-core coupling model

Both particle and collective degrees of freedom in $^{122}$Te are considered in the PCM [37] by treating the nucleus as two proton particles coupled to a vibrational core. This nucleus has been examined previously using the PCM [6,38]. We examine $^{122}$Te levels using the code PPCORE [37,39,40] in light of our new level and transition-rate information.

The PCM Hamiltonian used for these calculations is

$$H = \sum_{\lambda\mu}\hbar\omega_\lambda\left(b^\dagger_{\lambda\mu}b_{\lambda\mu}+\frac{1}{2}\right)+\sum_p\epsilon_p c^\dagger_p c_p + V_{pp} - \sum_{pq\lambda\mu}\sqrt{\frac{\pi}{2\lambda+1}}\xi_\lambda\hbar\omega_\lambda[b_{\lambda\mu}+(-1)^\mu b^\dagger_{\lambda-\mu}] \times\langle p|Y_{\lambda\mu}|q\rangle c^\dagger_p c_p, \quad (4)$$

where $c_p$ and $c^\dagger_p$ are the particle annihilation and creation operators, $b_p$ and $b^\dagger_p$ are the phonon annihilation and creation operators, $\epsilon_p$ are the single-particle energies, and $V_{pp}$ is the fermion-fermion interaction, which is taken to be a surface-delta interaction. The particle-phonon interaction strengths are defined as $\xi_\lambda = \langle\frac{r\partial V}{\partial r}\rangle\beta_\lambda/(\sqrt{\pi}\hbar\omega_\lambda)$, the deformation is defined as $\beta_\lambda = B(E\lambda;0^+_1\rightarrow\lambda_1)[\frac{3ZeR_0^\lambda}{4\pi}]^{-2}$, $\hbar\omega_\lambda$ is the core phonon energy for $\lambda = (2, 3)$, and the surface stiffness parameter is given by $C_\lambda = \frac{(2\lambda+1)\hbar\omega_\lambda}{2\beta^2_\lambda}$.

The pairing strength $G$ between the two protons is predicted to have a value of $G = 17.05/A, 19.2/A - 7.4(N-Z)/A^2$, or 0.20 [40]. In this work, the best value of $G$ was determined by considering the goodness of fit to the 17 lowest excited levels after all other parameters were set consistent with model definitions, core phonon energies, and deformation parameters. The best value of $G$ found for each parameter set was within the range expected by predictions and is listed in Table V.

Level energies and reduced electromagnetic transition rates were calculated using the $1g_{7/2}$, $2d_{5/2}$, $1h_{11/2}$, $2d_{3/2}$, and $3s_{1/2}$ single-particle orbitals and values of $\langle r\partial V/\partial r\rangle$ of 30, 40, and 50 MeV. Consistently, $\langle r\partial V/\partial r\rangle = 50$ MeV was found to best represent the data and was the value used for all PCM calculations presented. Initial model calculations were made using particle-phonon interaction strengths deduced from the adopted values of the $^{120}$Sn core deformation parameters $\beta_2 = 0.1075$ [33] and $\beta_3 = 0.1370$ [41], and from the $^{120}$Sn $2^+_1$- and $3^-_1$-level energies of 1.17 and 2.40 MeV, respectively, which were taken as the $\hbar\omega_2$ and $\hbar\omega_3$ core phonon energies. The octupole phonon energy was adjusted to reproduce approximately the experimental $3^-_1$ energy, while $\hbar\omega_2$ was kept fixed. Parameters for all calculations, including the orbital energies [6,40,42], are given in Table V. Calculated energies for two different sets of single-particle energies are shown in Fig. 8, and the corresponding transition rates are given in Table II.

For all parameter sets, the model consistently underpredicts the energy of the $6^+_1$ state by overemphasizing the particle configurations. The PCM wave functions indicate approximately a 35% contribution to this state from the $(1g_{7/2})^2$ and $(2d_{5/2}, 1g_{7/2})$ two-proton configurations. The nearly constant energy of the $6^+_1$ state in the heavier Te nuclei is thought to be due to proton excitations dominating the wave function for this state [1,9]. It appears that in $^{122}$Te collective configurations are more important than the PCM predicts. Recent observations in $^{126}$Te support the strong role of proton particle configurations in the $6^+_1$ state in that nucleus, as the PCM calculations better reproduce the level energy [17].

Another problem with the model calculations is that the predicted $0^+$ level energies are too high compared to what is observed experimentally. The wave functions for each of these states are dominated by different configurations, so there is no obvious way to lower the $0^+$ energies. The levels appear to be outside the model space, which lends more support to an intruder-state interpretation for these states. A similar problem was observed previously with the quasiparticle phonon model, since that model also could not handle the intruder configurations in these levels [5]. With all parameter sets in Table V, the PCM does well reproduce the staggered order and energies observed in the second band.

Two different techniques were used to reproduce the experimental B($E2$; $2^+_1\rightarrow 0^+_1$) transition probability: (1) the effective charge $e_{\rm eff}$ was varied from its initial value of $e_{\rm eff} = e$, and (2) the stiffness parameter $C_2$ was varied while changing $\beta_2$ and $\xi_2$ to maintain model consistency. Differences in the level scheme were insignificant, but the transition rates changed for some levels. Electromagnetic transition rates from both methods are listed in Table II and parameter sets are listed in Table V.

No levels were removed from consideration in Fig. 8, so the corresponding experimental B($E2$) values for PCM

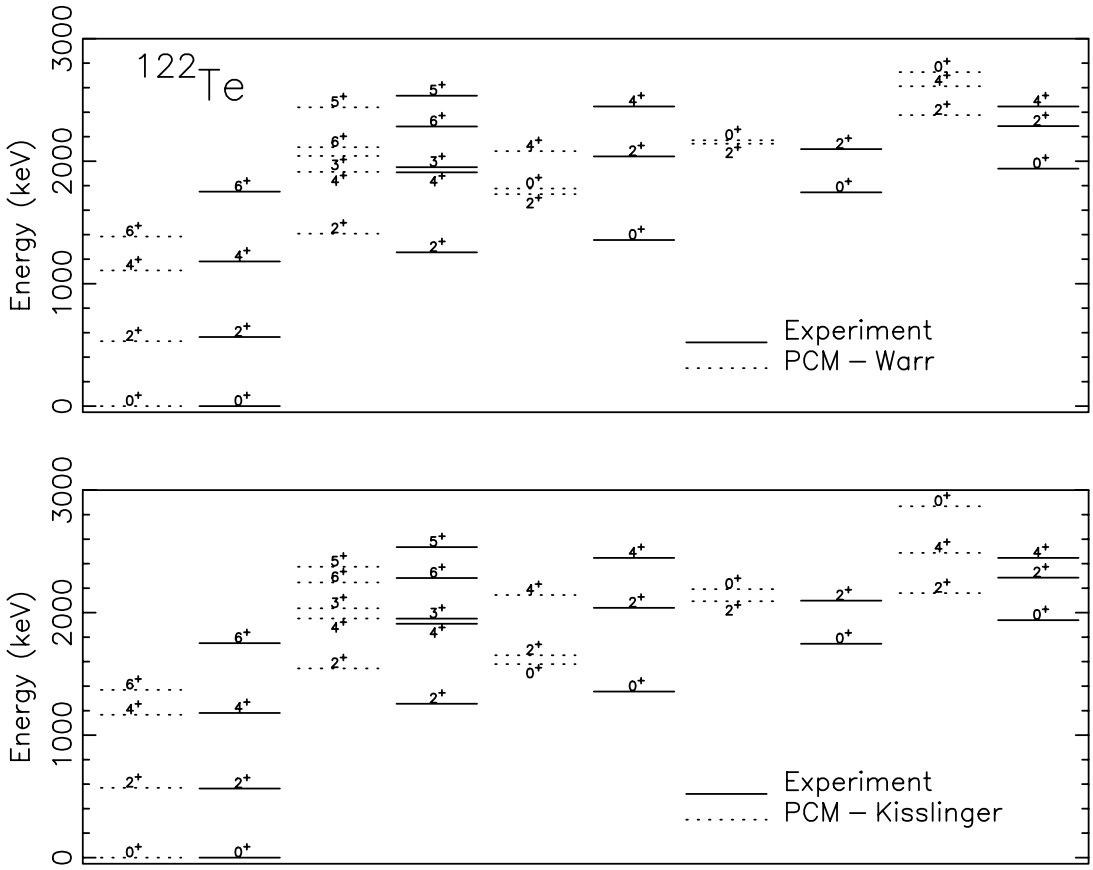


FIG. 8. Particle-core coupling model calculations for the Warr *et al*. [40] and Kisslinger and Sorensen [42] parameter sets listed in Table V.

model comparison in Table II are in the column labeled *with intruders*. The decay of most states in the $N_2$ band and the decay of the aforementioned $2_3^+$ level are very poorly described by the model. Comparison of the calculated rates to the experimental data with intruder states removed results in the same conclusion regarding levels in the $N_2$ band, but the calculated $2_3^+$ state decays better correspond to what is observed for the experimental $2_4^+$ state. For either data comparison, model transition rates agree rather well with those observed for a few levels, but in general the transition rates are not as well described as with the previously discussed IBM-2 calculations.

### E. Mixed-symmetry states

Excited levels for which the collective motion of neutrons and protons is distinguishable, or mixed-symmetry states (MS), have been observed in several nuclei in this region; see for example Refs. [43,44]. Signatures of MS strength in vibrational nuclei include decays from $2^+_{\rm MS}$ levels to the $2_1^+$ symmetric state with enhanced $M1$ transition rates and weak $E2$ transitions to the ground state [45]. Another characteristic of MS strength in vibrational nuclei is a small multipole-mixing ratio for decays between the $2^+_{\rm MS}$ and $2_1^+$ states [43,45]. Mixed-symmetry excitations have been investigated previously in this nucleus. In QPM calculations [5], the theoretical $2_3^+$ state has a strong MS component. Subber *et al*. [1] suggested that the $2_4^+$ state contained the MS strength, whereas Rikovska *et al*. [4] conclude that it is difficult to identify MS states in the Te nuclei because of the large role played by intruder configurations.

The lowest six $2^+$ states are observed in this work along with at least upper limits on transition rates for their decays. The B($M1$; $2_x^+ \rightarrow 2_1^+$) ($x = 2$–6) are shown in the left panels of Fig. 9, and B($E2$) values are shown for the decays from the same states into the $0_1^+$ (upper right) and the $2_1^+$ levels (lower right). The ground-state $E2$ decay is expected to be on the order of at most a few Weisskopf units [45]. The upper and lower left panels show the $M1$ rates calculated using the multipole-mixing ratio with the smallest $\chi^2$ value and the alternate solution, respectively.

Calculations completed using the IBM-2 with the *normal* parameters for $^{122}$Te from Ref. [4] indicate the MS strength is located primarily in the $2_3^+$ state. From these calculations the predicted $M1$ rates for transitions from $2^+$ levels into the first excited state are as follows: B($M1$; $2_2^+ \rightarrow 2_1^+$) $= 0.003\,\mu_N^2$, B($M1$; $2_3^+ \rightarrow 2_1^+$) $= 0.02\,\mu_N^2$, B($M1$; $2_4^+ \rightarrow 2_1^+$) $= 0.002\,\mu_N^2$, B($M1$; $2_5^+ \rightarrow 2_1^+$) $= 0.003\,\mu_N^2$, and B($M1$; $2_6^+ \rightarrow 2_1^+$) $= 0.002\,\mu_N^2$. These are compared with measured values of $0.012^{+6}_{-5}$, 0.006(1), 0.012(1), 0.012(1), and 0.002(6) $\mu_N^2$, respectively.

Experimentally, it appears that the $M1$ strength is uniformly distributed through the $2_2^+$, $2_4^+$, and $2_5^+$ states with the $2_3^+$ state having half the strength of the others, provided the smaller

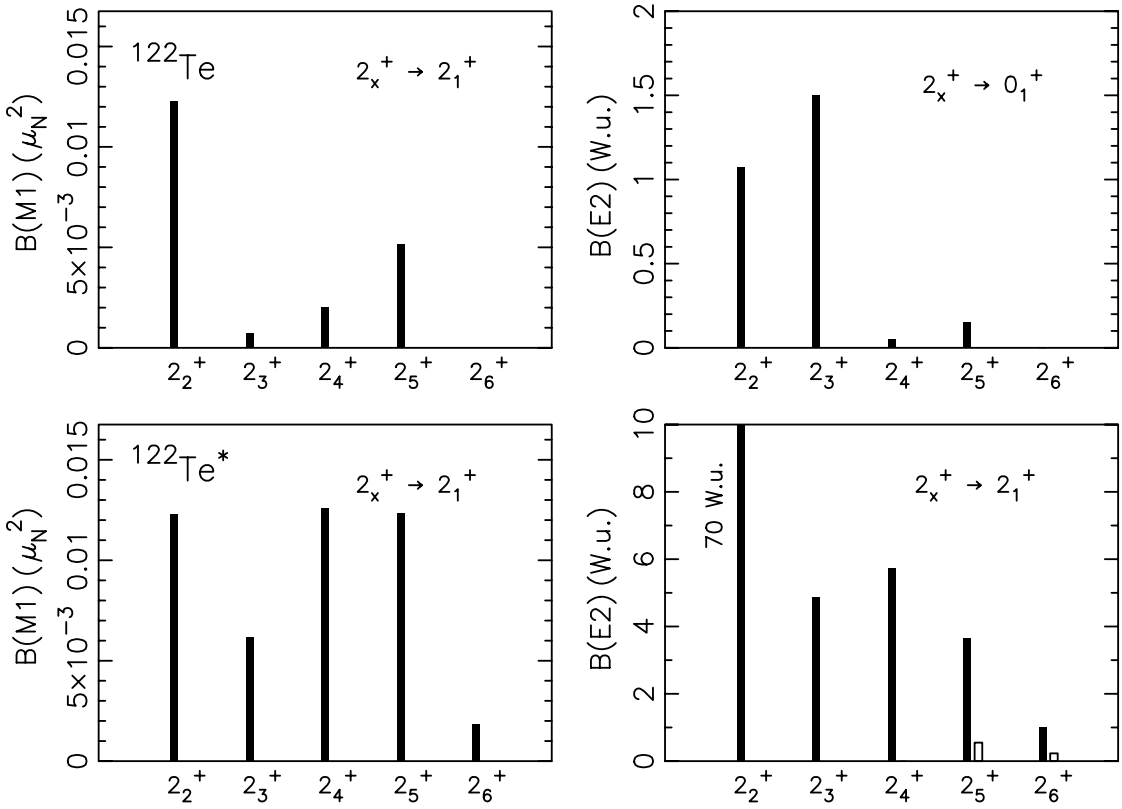


FIG. 9. B($M1$) and B($E2$) values for the $2_2^+$-$2_6^+$ states in $^{122}$Te. The left panels show B($M1$; $2_x^+ \rightarrow 2_1^+$) for $x = 2$–6. Values in the top left panel were calculated using the first multipole-mixing ratio listed for $2_x^+ \rightarrow 2_1^+$ in Table I; the bottom left panel shows the same values calculated with the alternate mixing ratio. The right panels show B($E2$; $2_x^+ \rightarrow 0_1^+$) and B($E2$; $2_x^+ \rightarrow 2_1^+$) for the same levels. For the B($E2$; $2_x^+ \rightarrow 2_1^+$) values, calculations from the first and second multipole-mixing ratios are shown side by side.

value of the multipole-mixing ratio is used. These $M1$ rates are not particularly fast for this mass region [46]. The summed $M1$ strength of 0.045 $\mu_N^2$ is about 44% of the predicted MS strength for this nucleus in the U(5) limit [45]. It appears that mixing with other configurations weakens the role of distinguishable neutron and proton collective excitations in this nucleus.

### F. Multiphonon structures

Coupling between single quadrupole and octupole vibrational modes, or quadrupole-octupole coupled (QOC) states, should produce a quintet of levels with spins $1^-$–$5^-$. In a simple vibrational model these states are predicted to lie at an energy given by the sum of $E(2_1^+)$ and $E(3_1^-)$, which is $\simeq$2760 keV in $^{122}$Te.

Candidates for these states have been identified in a few other nuclei in this mass region; some examples are in $^{112}$Cd [47], $^{144}$Sm [48], and $^{144}$Nd [49,50]. Ideally $E3$ transitions from this quintet of states to the $2_1^+$ and $E2$ transitions into the $3_1^-$ should have B($E3$) and B($E2$) values of the same strength as B($E3$; $3_1^- \rightarrow 0_1^+$) and B($E2$; $2_1^+ \rightarrow 0_1^+$), respectively [49]. In practice one usually cannot observe large $E3$ strength into the single phonon states. To identify candidates in $^{122}$Te, enhanced B($E2$) values, observed decay branches, and model calculations guide the assignments.

*QOC $1^-$ state.* The lowest $1^-$ QOC state candidate is at 2592.5 keV. This level was identified as a QOC state in Refs. [5,51] from comparisons with quasiparticle phonon model (QPM) calculations and from the identification of analogous $1^-$ states in $^{124}$Te at 2747 keV and in $^{126}$Te at 2974 keV. We have investigated all three of these nuclei using the $(n,n'\gamma)$ reaction, and the QOC $1^-$ state candidates are all found to exhibit strong decays to the ground state and are observed to have similar lifetimes of 26(2) fs, 42(3) fs (unpublished), and $39^{+4}_{-3}$ fs for $^{122}$Te, $^{124}$Te, and $^{126}$Te, respectively. The $1^-$ QOC state is predicted to decay by an $E1$ transition on the order of several milli-Weisskopf units to the ground state [51]. The parity of this level in $^{122}$Te remains in question, but if it is a $1^-$ level, a B($E1$; $1_1^- \rightarrow 0_1^+$) = 1 mW.u is observed, which agrees well with QPM predictions.

*QOC $2^-$ state.* Berendakov *et al.* [11] identify a state at 2636 keV as a $2^-$ QOC state candidate. A state at 2636 keV was observed in $(d, d')$ measurements, which does not support the unnatural parity assignment [5]. We see two levels at this energy based on the 2072.2- and 2073.7-keV doublet observed in the $\gamma$-$\gamma$ coincidence data, but no information was obtained to resolve the parity issue.

*QOC $3^-$ state.* A spin-3 level at 2801 keV is observed to decay into both the $2_1^+$ and $3_1^-$ states, although a definite parity for this state was not determined.

*QOC $4^-$ state*. The lowest identified $4^-$ state is at 2538.6 keV. Decays from this state to the $3_1^-$ state were not observed.

*QOC $5^-$ state*. The lowest $5^-$ state is observed at 2408.0 keV. Shell-model calculations indicate this state is formed by promoting $3s_{1/2}$ and $2d_{3/2}$ neutrons into $1h_{11/2}$ orbitals [52]. This state was weakly populated in proton stripping reactions and strongly populated in two-neutron pick-up reactions [20,52,53], which supports the idea that this level has strong two-neutron quasiparticle components, although the enhancement of the excitation of this state suggests it has collective strength as well [53]. The $5^-$ QOC state lies at 3048 keV according to QPM calculations [5]. A level is observed in this work at 3068.9 keV that decays into the $3_1^-$ with a B($E2$) $= 25 \pm 5$ W.u., which is a possible $5^-$ state and a candidate for a QOC state.

Clearly, definite parity information is needed for many of the observed levels in $^{122}$Te to understand more clearly the role of QOC states in this nucleus.

## V. SUMMARY

The level scheme and decay characteristics of $^{122}$Te to 3.3-MeV excitation have been determined using $\gamma$-ray detection following inelastic neutron scattering. Many new levels, transitions, and lifetimes for more than 70 levels were found from $\gamma$-ray excitation functions, angular distributions, $\gamma\gamma$ coincidences, and Doppler shifts. Prior to this investigation, only three lifetimes were known in this nucleus. Several low-lying $0^+$ levels were unambiguously identified.

The low-lying positive parity levels and many transition rates were well described by IBM-2 with intruder-state mixing calculations. Experimental evidence, including an in-band transition with a large B($E2$) value, was found to support intruder excitations and an emerging intruder band in this nucleus. When the IBM-2 model calculations are used to remove states with large intruder components, U(5) calculations reproduce the remaining level energies in what appears to be distinct 1-, 2-, 3-, and 4-quadrupole phonon states. Experimental B($E2$) rates agree with U(5) calculations for many transitions.

The PCM treats $^{122}$Te as two proton particles coupled to a $^{120}$Sn core. Calculations with this model reproduced some features of the low-lying spectrum, such as the staggering observed in the quasi-$\gamma$ band and some transition rates. The particle-like nature of the $6_1^+$ state observed for the higher mass Te nuclei does not appear to be as important in $^{122}$Te where the model seems to underemphasize the collective nature of the level and predicts too low an energy for that state. Additionally, the model does not produce enough low-lying $0^+$ states, nor does it predict the transition rates for most of the observed levels.

The neutron-proton MS strength seems to be fairly evenly divided among the $2_2^+$, $2_3^+$, $2_4^+$, and $2_5^+$ levels since each of these has about the same $M1$ strength into the $2_1^+$ state. The summed strength is about 40% of what is predicted for a vibrational nucleus, which may mean that mixing with intruder and quasiparticle configurations depletes the MS strength.

Finally, QOC state candidates were identified, but many of the levels do not have well-defined parities, nor do they exhibit the transition rates to lower levels expected from such states. The QOC strength appears to be fragmented and to be mixed with other configurations much like the observed MS strength.

## ACKNOWLEDGMENTS

The support of the National Science Foundation for this project through Grant Nos. PHY-9600431, PHY-9626846, and PHY-0098813 is gratefully acknowledged. Additionally, we would like to thank the O'Hara Foundation at the University of Dallas for summer support for students.

[1] A. Subber, W. D. Hamilton, P. Park, and K. Kumar, J. Phys. G **13**, 161 (1987).
[2] J. Kern, P. E. Garrett, J. Jolie, and H. Lehmann, Nucl. Phys. **A593**, 21 (1995).
[3] A. Aprahamian, D. S. Brenner, R. F. Casten, R. L. Gill, and A. Piotrowski, Phys. Rev. Lett. **59**, 535 (1987).
[4] J. Rikovska, N. J. Stone, P. M. Walker, and W. B. Walters, Nucl. Phys. **A505**, 145 (1989).
[5] W. Schauer, C. Doll, T. von Egidy, R. Georgii, J. Ott, H.-F. Wirth, A. Gollwitzer, G. Graw, R. Hertenberger, B. Valnion, M. Grinberg, and Ch. Stoyanov, Nucl. Phys. **A652**, 339 (1999), and references therein.
[6] V. Lopac, Nucl Phys. **A155**, 513 (1970)
[7] A. Kerek, Nucl. Phys. **A176**, 466 (1971).
[8] J. Rikovska, N. J. Stone, and W. B. Walters, Phys. Rev. C **36** 2162, (1987).
[9] C. S. Lee, J. A. Cizewski, D. Barker, R. Tanczyn, G. Kumbartzki, J. Szczepanski, J. W. Gan, H. Dorsett, R. G. Henry, and L. P. Farris, Nucl. Phys. **A528**, 381 (1991).
[10] T. Tamura, Nucl. Data Sheets **71**, 461 (1994).
[11] S. A. Berendakov, L. I. Govor, A. M. Demidov, and I. V. Mikhaĭlov, Sov. J. Nucl. Phys. **52**, 3 (1990).
[12] A. M. Demidov and I. V. Mikhaĭlov, Sov. J. Nucl. Phys. **53**, 5 (1991).
[13] C. A. McGrath, P. E. Garrett, M. F. Villani, and S. W. Yates, Nucl. Instrum. Methods A **421**, 458 (1999).
[14] P. E. Garrett, N. Warr, and S. W. Yates, J. Res. Natl. Inst. Stand. Technol. **105**, 141 (2000), and references therein.
[15] E. Sheldon and D. M. van Patter, Rev. Mod. Phys. **38**, 143 (1966).
[16] R. W. Harper, T. W. Godfrey, and J. L. Weil, Phys. Rev. C **26**, 1432 (1982).
[17] J. R. Vanhoy, J. A. Tanyi, K. A. Crandell, T. H. Churchill, S. F. Hicks, M. C. Burns, P. A. Roddy, N. V. Warr, T. B. Brown, and S. R. Lesher, Phys. Rev. C **69**, 064323 (2004).
[18] T. Belgya, G. Molnar, and S. W. Yates, Nucl. Phys. **A607**, 43 (1996).
[19] K. B. Winterbon, Nucl. Phys. **A246**, 293 (1975).
[20] R. L. Auble and J. B. Ball, Nucl. Phys. **A179**, 353 (1972).

[21] P. M. Walker, C. J. Ashworth, I. S. Grant, V. R. Green, J. Rikovska, T. L. Shaw, and N. J. Stone, J. Phys. G **13**, L195 (1987).
[22] J. Barrette, M. Barrette, R. Haroutunian, G. Lamoureux, and S. Monaro, Phys. Rev. C **10**, 1166 (1974).
[23] M. Kadi, N. Warr, P. E. Garrett, J. Jolie, and S. W. Yates, Phys. Rev. C **68**, 031306(R) (2003).
[24] J. Kumpulainen, R. Julin, J. Kantele, A. Passoja, W. H. Trzaska, E. Verho, J. Vaaramaki, D. Cutoiu, and M. Ivascu, Phys. Rev. C **45**, 640 (1992).
[25] D. C. Radford, A. Galindo-Uribarri, G. Hackman, and V. P. Janzen, Nucl. Phys. **A557**, 311 (1993).
[26] M. Schimmer, R. Wirowski, S. Albers, G. Bohm, A. Dewald, A. Gelberg, and P. von Brentano, Z. Phys. A **338**, 117 (1991).
[27] E. S. Paul, C. W. Beausang, S. A. Forbes, S. J. Gale, A. N. James, P. M. Jones, M. J. Joyce, R. M. Clark, K. Hauschild, I. M. Hibbert, R. Wadsworth, R. A. Cunningham, J. Simpson, T. Davinson, R. D. Page, P. J. Sellin, P. J. Woods, D. B. Fossan, D. R. LaFosse, H. Schnare, M. P. Waring, A. Gizon, and J. Gizon, Phys. Rev. C **48**, R490 (1993).
[28] J. R. Vanhoy, R. T. Coleman, K. A. Crandell, S. F. Hicks, B. A. Sklaney, M. M. Walbran, N. V. Warr, J. Jolie, F. Corminboeuf, L. Genilloud, J. Kern, J.-L. Schenker, and P. E. Garrett, Phys. Rev. C **68**, 034315 (2003).
[29] E. S. Paul, C. W. Beausang, S. A. Forbes, S. J. Gale, A. N. James, P. M. Jones, M. J. Joyce, H. R. Andrews, V. P. Janzen, D. C. Radford, D. Ward, R. M. Clark, K. Hauschild, I. M. Hibbert, R. Wadsworth, R. A. Cunningham, J. Simpson, T. Davinson, R. D. Page, P. J. Sellin, P. J. Woods, D. B. Fossan, D. R. LaFosse, H. Schnare, M. P. Waring, A. Gizon, J. Gizon, T. E. Drake, J. DeGraaf, and S. Pilotte, Phys. Rev. C **50**, 698 (1994).
[30] M. Sambataro, Nucl. Phys. **A380**, 365 (1982).
[31] T. Otsuka and N. Yoshida, Japanese Atomic Energy Research Institute Report 85-094 (1985) (unpublished).
[32] P. D. Duval and B. R. Barrett, Nucl. Phys. **A376** 213 (1982).
[33] S. Raman, C. W. Nestor, Jr., and P. Tikkanen, At. Data Nucl. Data Tables **78**, 1 (2001).
[34] T. Belgya, B. Fazekas, G. Molnár, R. A. Gatenby, E. L. Johnson, E. M. Baum, D. Wang, D. P. DiPrete, and S. W. Yates, in *Proceedings of the 8th International Symposium on Capture γ-Ray Spectroscopy and Related Topics, Fribourg, Switzerland, 1993*, edited by J. Kern (World Scientific, Singapore, 1994), p. 878.
[35] P. Cejnar, J. Jolie, and J. Kern, Phys. Rev. C **63**, 047304 (2001).
[36] O. Scholten, in *Computational Nuclear Physics 1: Nuclear Structure*, edited by K. Langanke, J. A. Maruhn, and S. Koonin (Springer-Verlag, New York, 1991), p. 88.
[37] K. Heyde and P. J. Brussard, Nucl. Phys. **A104**, 81 (1967).
[38] E. Degrieck and G. Van den Berghe, Nucl. Phys. **A231**, 141 (1974).
[39] J. Copnell, S. J. Robinson, J. Jolie, and K. Heyde, Phys. Rev. C **46**, 1301 (1992).
[40] N. Warr, S. Drissi, P. E. Garrett, J. Jolie, J. Kern, H. Lehman, S. J. Mannanal, and J.-P. Vorlet, Nucl. Phys. **636**, 379 (1998), and references therein.
[41] T. Kibédi and R. H. Spear, At. Data Nucl. Data Tables **80**, 35 (2002).
[42] L. S. Kisslinger and R. A. Sorensen, Rev. Mod. Phys. **35**, 835 (1963).
[43] P. E. Garrett, H. Lehmann, C. A. McGrath, M. Yeh, and S. W. Yates, Phys. Rev. C **54**, 2259 (1996).
[44] D. Bandyopadhyay, C. C. Reynolds, C. Fransen, N. Boukharouba, M. T. McEllistrem, and S. W. Yates, Phys. Rev. C **67**, 034319 (2003).
[45] F. Iachello, Phys. Rev. Lett. **53**, 1427 (1984).
[46] P. M. Endt, At. Data Nucl. Data Tables, **26**, 47 (1981).
[47] P. E. Garrett, H. Lehmann, J. Jolie, C. A. McGrath, M. Yeh, and S. W. Yates, Phys. Rev. C **59**, 2455 (1999).
[48] R. A. Gatenby, J. R. Vanhoy, E. M. Baum, E. L. Johnson, S. W. Yates, T. Belgya, B. Fazekas, Á. Veres, and G. Molnár, Phys. Rev C **41**, R414 (1990).
[49] S. J. Robinson, J. Jolie, H. G. Börner, P. Schillebeeckx, S. Ulbig, and K. P. Lieb, Phys. Rev. Lett. **73**, 412 (1994).
[50] S. F. Hicks, C. M. Davoren, W. M. Faulkner, and J. R. Vanhoy, Phys. Rev. C **57**, 2264 (1998).
[51] R. Schwengner, G. Winter, W. Schauer, M. Grinberg, F. Becker, P. von Brentano, J. Eberth, J. Enders, T. von Egidy, R.-D. Herzberg, N. Huxel, L. Käubler, P. von Neumann-Cosel, N. Nicolay, J. Ott, N. Pietralla, H. Prade, S. Raman, J. Reif, A. Richter, C. Schlegel, H. Schnare, T. Servene, S. Skoda, T. Steinhardt, C. Stoyanov, H. G. Thomas, I. Wiedenhöver, and A. Zilges, Nucl. Phys. **A620**, 277 (1997).
[52] P. Nesci, R. Smith, K. Amos, and H. V. Geramb, Aust. J. Phys. **28**, 659 (1975).
[53] M. Matoba, M. Hyakutake, K. Yagi, Y. Aoki, and C. Rangacharyulu, Nucl. Phys. **A261**, 223 (1976).